ELASTIC ANISOTROPY OF HCP METAL CRYSTALS AND POLYCRYSTALS

Desmond Tromans
Department of Materials Engineering, University of British Columbia, Vancouver BC, Canada V6T 1Z4
E-mail: dtromans@interchange.ubc.ca

ABSTRACT

The monocrystal elastic behaviours of twenty four hexagonal close packed (HCP) metals at room temperature are reviewed based on published values of their monocrystal elastic constants. In particular, the angular variation of the Young's Modulus (*E*) and the Rigidity (Shear) Modulus (*G*) are determined using general equations developed by Voigt [1928] and comparisons between the different metals presented graphically. The consequences of anisotropic monocrystal behaviour on the elastic behaviour of polycrystals composed of randomly oriented grains (crystal aggregates) are explored using a three dimensional spherical analysis together with the analytical methods of Voigt [1889] and Reuss [1929], and comments made on the consequences of non-randomly oriented grains.

Keywords: *Matrices*, *stiffness, compliance*, *Young's modulus, shear modulus, texture.*

1. INTRODUCTION

There is considerable experimental information on the elastic constants of metal monocrystals and mineral crystals. However, a comparative examination of behaviour between all HCP metals stable at room temperature, particularly a single source graphical comparison, is both desirable and useful. The physics upon which elastic constants are based and the relationships between the constants and crystallography are well established. However, the language of crystal physics is somewhat complex, involving conventions and procedures which are not immediately obvious to the non-specialist. Consequently, some general comments relating to the basic terminologies of stresses and strains, tensors and matrices, and crystal structure are presented first, followed by an examination of the elastic behaviour of HCP monocrystals and subsequent effects on polycrystals.

2. BASIC TERMINOLOGY

2.1. Stress and Strain.

Consider a stressed cube of metal crystal where the normal to the cube faces are parallel to cube edges having orthogonal axial directions X_1, X_2 and X_3, as shown in Figure 1.

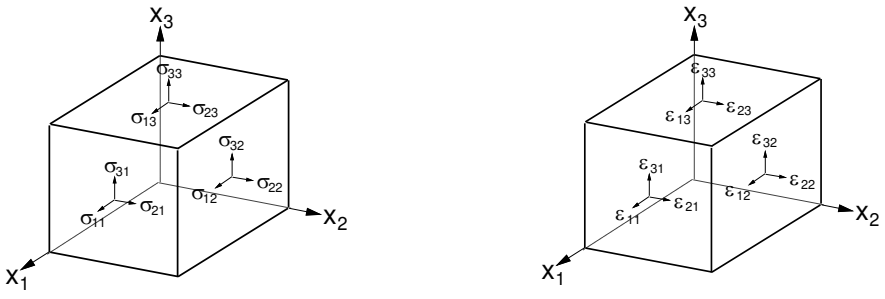

Figure 1. (a) Stress notation; (b) Strain notation.

Stresses σ and strains ε are identified by means of two subscripts which for convenience will be identified as *i* and *j* for stresses σ_{ij}, and *k* and *l* for strains ε_{kl}, with each subscript having a value 1, 2 or 3. Considering stresses, the first subscript *i* denotes the axial direction X_i of the force transmitted across the cube face and the second subscript *j* denotes the axial direction X_j of the normal to the cube face. Thus, referring to Fig. 1a, σ_{11}, $\sigma_{22}$and σ_{33} (*i.e.* σ_{ii})) are the normal tensile stress components parallel to the X_1, X_2 and X_3 axes, respectively and σ_{13} σ_{23}, $\sigma_{21,}$ $\sigma_{31,}$ σ_{12} and σ_{32} (*i.e.* σ_{ij})) are shear stresses lying in the plane normal to X_j. For tensile strains the subscripts *k* and *l* also have a value 1, 2 or 3 and denote the axial direction X_k of the strain (extension) and the axial direction X_l of the tensile

force. Consequently, referring to Fig. 1b, ε_{11}, ε_{22} and ε_{33} (i.e. ε_{kk}) are tensile strains (fractional extensions) parallel to the X_1, X_2 and X_3 axes, respectively. The shear strains ε_{kl} are due to a rotation towards the X_k axis of a line element parallel to the X_l axis. For example, ε_{23} indicates a rotation towards the X_2 axis of a line element parallel to the X_3 axis, which obviously involves a rotation about the third axis X_1

.

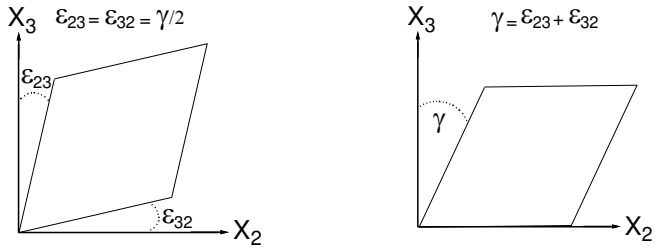

(a) (b)

Figure. 2. Relationship between (a) tensor shear strain pairs and (b) engineering shear strain γ.

The shear strains are angles measured in radians. For example, if a pure shear stress (torque) is applied to cause a rotation about the X_1 axis the resulting pure shear strains ε_{23} and ε_{32} are shown in Fig. 2. Note that the engineering shear strain γ is the sum of the shear strains $\varepsilon_{23} + \varepsilon_{32}$. The consequences of this are discussed later in relation to compliances.

2.2. Elastic Stiffness and Compliance.

Elastic materials exhibit a proportional relationship between an applied stress σ and the resulting tensile strain ε, provided the strains are small. The resulting linear relationship is known as Hooke's Law. In engineering, the constant of proportionality is known as the tensile elastic modulus E (Young's Modulus) and the usual form of the relationship is given by Eq. (1) where σ is a uniaxial stress and ε is the strain elongation in the direction of the applied stress:

$$\sigma = E\varepsilon \tag{1}$$

In fact, Equation 1 describes a uniaxial stress situation with three dimensional strains (elongation strain plus lateral strains dependent upon Poisson's ratio) and is more formally stated in elasticity in terms of the compliance S with ε as the dependent variable:

$$\varepsilon = S\sigma \tag{2}$$

where S is the reciprocal Young's Modulus ($1/E$).

In analogous manner, a three dimensional stress situation with uniaxial strain is expressed in terms of the stiffness C with the stress in the direction of uniaxial strain being the dependent variable:

$$\sigma = C\varepsilon \tag{3}$$

2.3. Tensors and Matrices.

Note that in general $C \neq E$. and the elastic relationship between stresses and strains in crystals must be stated in a more generalized manner:

$$\sigma_{ij} = C_{ijkl}\varepsilon_{kl} \quad \text{and} \quad \varepsilon_{kl} = S_{klij}\sigma_{ij} \tag{4}$$

In Eq. (4), C_{ijkl} are stiffness constants of the crystal and S_{klij} are the compliances of the crystal and both are a fourth rank tensor (Wooster, 1949; Nye, 1985). Figure 1 shows there are nine forms of σ_{ij} and nine forms of ε_{kl} so that the generalized Eq. (4) leads to 81 C_{ijkl} stiffness coefficients and 81 S_{klij} compliance coefficients which form a fourth rank tensor represented by a symmetrical 9 x 9 array of coefficients. Thus, Eq. (4) becomes:

Full tensor notation *Full tensor notation*

$$\begin{bmatrix}\sigma_{11}\\ \sigma_{22}\\ \sigma_{33}\\ \sigma_{23}\\ \sigma_{31}\\ \sigma_{12}\\ \sigma_{32}\\ \sigma_{13}\\ \sigma_{21}\end{bmatrix} = \begin{bmatrix} C_{1111} & C_{1122} & C_{1133} & C_{1123} & C_{1131} & C_{1112} & C_{1132} & C_{1113} & C_{1121}\\ C_{2211} & C_{2222} & C_{2233} & C_{2223} & C_{2231} & C_{2212} & C_{2232} & C_{2213} & C_{2221}\\ C_{3311} & C_{3322} & C_{3333} & C_{3323} & C_{3331} & C_{3312} & C_{3332} & C_{3313} & C_{3321}\\ C_{2311} & C_{2322} & C_{2333} & C_{2323} & C_{2331} & C_{2312} & C_{2332} & C_{2313} & C_{2321}\\ C_{3111} & C_{3122} & C_{3133} & C_{3123} & C_{3131} & C_{3112} & C_{3132} & C_{3113} & C_{3121}\\ C_{1211} & C_{1222} & C_{1233} & C_{1223} & C_{1231} & C_{1212} & C_{1232} & C_{1213} & C_{1221}\\ C_{3211} & C_{3222} & C_{3233} & C_{3223} & C_{3231} & C_{3212} & C_{3232} & C_{3213} & C_{3221}\\ C_{1311} & C_{1322} & C_{1333} & C_{1323} & C_{1331} & C_{1312} & C_{1332} & C_{1313} & C_{1321}\\ C_{2111} & C_{2122} & C_{2133} & C_{2123} & C_{2131} & C_{2112} & C_{2132} & C_{2113} & C_{2121}\end{bmatrix}\begin{bmatrix}\varepsilon_{11}\\ \varepsilon_{22}\\ \varepsilon_{33}\\ \varepsilon_{23}\\ \varepsilon_{31}\\ \varepsilon_{12}\\ \varepsilon_{32}\\ \varepsilon_{13}\\ \varepsilon_{21}\end{bmatrix} \quad \begin{bmatrix}\varepsilon_{11}\\ \varepsilon_{22}\\ \varepsilon_{33}\\ \varepsilon_{23}\\ \varepsilon_{31}\\ \varepsilon_{12}\\ \varepsilon_{32}\\ \varepsilon_{13}\\ \varepsilon_{21}\end{bmatrix} = \begin{bmatrix} S_{1111} & S_{1122} & S_{1133} & S_{1123} & S_{1131} & S_{1112} & S_{1132} & S_{1113} & S_{1121}\\ S_{2211} & S_{2222} & S_{2233} & S_{2223} & S_{2231} & S_{2212} & S_{2232} & S_{2213} & S_{2221}\\ S_{3311} & S_{3322} & S_{3333} & S_{3323} & S_{3331} & S_{3312} & S_{3332} & S_{3313} & S_{3321}\\ S_{2311} & S_{2322} & S_{2333} & S_{2323} & S_{2331} & S_{2312} & S_{2332} & S_{2313} & S_{2321}\\ S_{3111} & S_{3122} & S_{3133} & S_{3123} & S_{3131} & S_{3112} & S_{3132} & S_{3113} & S_{3121}\\ S_{1211} & S_{1222} & S_{1233} & S_{1223} & S_{1231} & S_{1212} & S_{1232} & S_{1213} & S_{1221}\\ S_{3211} & S_{3222} & S_{3233} & S_{3223} & S_{3231} & S_{3212} & S_{3232} & S_{3213} & S_{3221}\\ S_{1311} & S_{1322} & S_{1333} & S_{1323} & S_{1331} & S_{1312} & S_{1332} & S_{1313} & S_{1321}\\ S_{2111} & S_{2122} & S_{2133} & S_{2123} & S_{2131} & S_{2112} & S_{2132} & S_{2113} & S_{2121}\end{bmatrix}\begin{bmatrix}\sigma_{11}\\ \sigma_{22}\\ \sigma_{33}\\ \sigma_{23}\\ \sigma_{31}\\ \sigma_{12}\\ \sigma_{32}\\ \sigma_{13}\\ \sigma_{21}\end{bmatrix} \tag{5}$$

The physical meaning of each C_{ijkl} is obtained by considering a set of applied stress components where all components of strain vanish except for either one normal component or a pair of shear components. An example with one normal component of strain is $\sigma_{11} = C_{1111}\varepsilon_{11}$ (*i.e.* $\sigma_{ii} = C_{ii}\varepsilon_{kk}$ where $i = k$). A situation corresponding to one pair of tensor shear components is $\sigma_{23} = C_{2323}\varepsilon_{23} + C_{2332}\varepsilon_{32}$ (where $i \neq j$, $k \neq l$) Similarly, the meaning of each S_{ijkl} is obtained by considering a set of applied strain components where all components of stress vanish except for either one normal component or a pair of shear components. An example with one normal component of stress is given by the situation where $\varepsilon_{11} = S_{1111}\sigma_{11}$ (*i.e.* $\varepsilon_{ii} = S_{ii}\varepsilon_{kk}$ where $i = k$). The situation corresponding to one pair of shear stress components is given by $\varepsilon_{23} = S_{2323}\sigma_{23} + S_{2332}\sigma_{32}$ (where $i \neq j$, $k \neq l$).

The number of suffixes on the stiffness and compliance may be decreased by considering the static equilibrium of a stressed cube in Fig. 1. It is evident that $\sigma_{12} = \sigma_{21}$, $\sigma_{13} = \sigma_{31}$ and $\sigma_{23} = \sigma_{32}$ otherwise rotations occur. Similarly, $\varepsilon_{12} = \varepsilon_{21}$, $\varepsilon_{13} = \varepsilon_{31}$ and $\varepsilon_{32} = \varepsilon_{23}$. The ability to interchange suffixes i and j in σ_{ij}, and suffixes k and l in ε_{kl}, implies that it is unnecessary to distinguish between i and j or between k and l (*e.g.* $\sigma_{23} = \sigma_{32}$, $\varepsilon_{12} = \varepsilon_{21}$). Consequently, following from Voigt [1928)], it has become common practice to use a contracted matrix notation with single number suffixes instead of pairs. The relationship between pairs (ij or kl) and single numbers (m or n) is shown below:

ij or kl	11	22	33	23,32	31,13	12,21
	↓	↓	↓	↓	↓	↓
m or n	1	2	3	4	5	6

Equation (5) may now be rewritten as Eq. (6) in the contracted tensor notation where the engineering shear strain $\gamma_{23} = (\varepsilon_{23}+\varepsilon_{32})$, $\gamma_{31} = (\varepsilon_{31}+\varepsilon_{13})$ and $\gamma_{12} = (\varepsilon_{12}+\varepsilon_{11})$, according to Fig. 2. Also, using the contracted notation $\sigma_{11}\rightarrow\sigma_1$, $\sigma_{22}\rightarrow\sigma_2$, $\sigma_{33}\rightarrow\sigma_3$, $\sigma_{23}\rightarrow\sigma_4$, $\sigma_{31}\rightarrow\sigma_5$, $\sigma_{12}\rightarrow\sigma_6$, $\sigma_{23}\rightarrow\sigma_4$; $\varepsilon_{11}\rightarrow\varepsilon_1$, $\varepsilon_{22}\rightarrow\varepsilon_2$, $\varepsilon_{33}\rightarrow\varepsilon_3$, $\gamma_{23}\rightarrow\gamma_4$, $\gamma_{32}\rightarrow\gamma_4$, $\gamma_{31}\rightarrow\gamma_5$, and . $\gamma_{12}\rightarrow\gamma_6$.

Contracted tensor notation *Contracted tensor notation*

$$\begin{bmatrix}\sigma_1\\ \sigma_2\\ \sigma_3\\ \sigma_4\\ \sigma_5\\ \sigma_6\end{bmatrix} = \begin{bmatrix} C_{11}\ C_{12}\ C_{13}\ C_{14}\ C_{15}\ C_{16}\ C_{14}\ C_{15}\ C_{16}\\ C_{12}\ C_{22}\ C_{23}\ C_{24}\ C_{25}\ C_{26}\ C_{24}\ C_{25}\ C_{26}\\ C_{13}\ C_{23}\ C_{33}\ C_{34}\ C_{35}\ C_{36}\ C_{34}\ C_{35}\ C_{36}\\ C_{14}\ C_{24}\ C_{34}\ C_{44}\ C_{45}\ C_{46}\ C_{44}\ C_{45}\ C_{46}\\ C_{15}\ C_{25}\ C_{35}\ C_{45}\ C_{55}\ C_{56}\ C_{45}\ C_{55}\ C_{56}\\ C_{16}\ C_{26}\ C_{36}\ C_{46}\ C_{56}\ C_{66}\ C_{46}\ C_{56}\ C_{66}\\ C_{14}\ C_{24}\ C_{34}\ C_{44}\ C_{45}\ C_{46}\ C_{44}\ C_{45}\ C_{46}\\ C_{15}\ C_{25}\ C_{35}\ C_{45}\ C_{55}\ C_{56}\ C_{45}\ C_{55}\ C_{56}\\ C_{16}\ C_{26}\ C_{36}\ C_{46}\ C_{56}\ C_{66}\ C_{46}\ C_{56}\ C_{66}\end{bmatrix}\begin{bmatrix}\varepsilon_1\\ \varepsilon_2\\ \varepsilon_3\\ \gamma_4/2\\ \gamma_5/2\\ \gamma_6/2\\ \gamma_4/2\\ \gamma_5/2\\ \gamma_6/2\end{bmatrix} \qquad \begin{bmatrix}\varepsilon_1\\ \varepsilon_2\\ \varepsilon_3\\ \gamma_4/2\\ \gamma_5/2\\ \gamma_6/2\\ \gamma_4/2\\ \gamma_5/2\\ \gamma_6/2\end{bmatrix} = \begin{bmatrix} S_{11}\ S_{12}\ S_{13}\ S_{14}\ S_{15}\ S_{16}\ S_{14}\ S_{15}\ S_{16}\\ S_{12}\ S_{22}\ S_{23}\ S_{24}\ S_{25}\ S_{26}\ S_{24}\ S_{25}S_{26}\\ S_{13}\ S_{23}\ S_{33}\ S_{34}\ S_{35}\ S_{36}\ S_{34}\ S_{35}S_{36}\\ S_{14}\ S_{24}\ S_{34}\ S_{44}\ S_{45}\ S_{46}\ S_{44}\ S_{45}S_{46}\\ S_{15}\ S_{25}\ S_{35}\ S_{45}\ S_{55}\ S_{56}\ S_{45}\ S_{55}S_{56}\\ S_{16}\ S_{26}\ S_{36}\ S_{46}\ S_{56}\ S_{66}\ S_{46}\ S_{56}S_{66}\\ S_{14}\ S_{24}\ S_{34}\ S_{44}\ S_{45}\ S_{46}\ S_{44}\ S_{45}S_{46}\\ S_{15}\ S_{25}\ S_{35}\ S_{45}\ S_{55}\ S_{56}\ S_{45}\ S_{55}S_{56}\\ S_{16}\ S_{26}\ S_{36}\ S_{46}\ S_{56}\ S_{66}\ S_{46}\ S_{56}\ S_{66}\end{bmatrix}\begin{bmatrix}\sigma_1\\ \sigma_2\\ \sigma_3\\ \sigma_4\\ \sigma_5\\ \sigma_6\\ \sigma_4\\ \sigma_5\\ \sigma_6\end{bmatrix} \qquad (6)$$

After summing each tensor equation represented in Eq. (6) it becomes evident that all the relationships between stresses, strains, and stiffness coefficients, and strains, stresses and compliance coefficients, may each be represented by a symmetrical 6x6 matrix as shown in Eq. (7):

C- Matrix *S- Matrix* *S-Matrix, ϕ-factors included*

$$\begin{bmatrix}\sigma_1\\ \sigma_2\\ \sigma_3\\ \sigma_4\\ \sigma_5\\ \sigma_6\end{bmatrix} = \begin{bmatrix} C_{11}\ C_{12}\ C_{13}\ C_{14}\ C_{15}\ C_{16}\\ C_{12}\ C_{22}\ C_{23}\ C_{24}\ C_{25}\ C_{26}\\ C_{13}\ C_{23}\ C_{33}\ C_{34}\ C_{35}\ C_{36}\\ C_{14}\ C_{24}\ C_{34}\ C_{44}\ C_{45}\ C_{46}\\ C_{15}\ C_{25}\ C_{35}\ C_{45}\ C_{55}\ C_{56}\\ C_{16}\ C_{26}\ C_{36}\ C_{46}\ C_{56}\ C_{66}\end{bmatrix}\begin{bmatrix}\varepsilon_1\\ \varepsilon_2\\ \varepsilon_3\\ \gamma_4\\ \gamma_5\\ \gamma_6\end{bmatrix} \qquad \begin{bmatrix}\varepsilon_1\\ \varepsilon_2\\ \varepsilon_3\\ \gamma_4\\ \gamma_5\\ \gamma_6\end{bmatrix} = \begin{bmatrix} S_{11}\ S_{12}\ S_{13}\ 2S_{14}\ 2S_{15}\ 2S_{16}\\ S_{12}\ S_{22}\ S_{23}\ 2S_{24}\ 2S_{25}\ 2S_{26}\\ S_{13}\ S_{23}\ S_{33}\ 2S_{34}\ 2S_{35}\ 2S_{36}\\ 2S_{14}\ 2S_{24}\ 2S_{34}\ 4S_{44}\ 4S_{45}\ 4S_{46}\\ 2S_{15}\ 2S_{25}\ 2S_{35}\ 4S_{45}\ 4S_{55}\ 4S_{56}\\ 2S_{16}\ 2S_{26}\ 2S_{36}\ 4S_{46}\ 4S_{56}\ 4S_{66}\end{bmatrix}\begin{bmatrix}\sigma_1\\ \sigma_2\\ \sigma_3\\ \sigma_4\\ \sigma_5\\ \sigma_6\end{bmatrix} \qquad \begin{bmatrix}\varepsilon_1\\ \varepsilon_2\\ \varepsilon_3\\ \gamma_4\\ \gamma_5\\ \gamma_6\end{bmatrix} = \begin{bmatrix} S_{11}\ S_{12}\ S_{13}\ S_{14}\ S_{15}\ S_{16}\\ S_{12}\ S_{22}\ S_{23}\ S_{24}\ S_{25}\ S_{26}\\ S_{13}\ S_{23}\ S_{33}\ S_{34}\ S_{35}\ S_{36}\\ S_{14}\ S_{24}\ S_{34}\ S_{44}\ S_{45}\ S_{46}\\ S_{15}\ S_{25}\ S_{35}\ S_{45}\ S_{55}\ S_{56}\\ S_{16}\ S_{26}\ S_{36}\ S_{46}\ S_{56}\ S_{66}\end{bmatrix}\begin{bmatrix}\sigma_1\\ \sigma_2\\ \sigma_3\\ \sigma_4\\ \sigma_5\\ \sigma_6\end{bmatrix} \qquad (7)$$

When the pairs of suffixes mn on the matrix shear compliances, S_{mn} are such that m or n are both 4, 5, or 6 the compliance S_{mn} is multiplied by a factor (ϕ) of 4 (*e.g.* $4S_{45}$, and $4S_{56}$). When either m or n are 4, 5, or 6 the compliance S_{mn} is multiplied by a factor (ϕ) of 2 (*e.g.* $2S_{16}$, $2S_{35}$, $2S_{24}$). All other compliances have a multiplying factor of unity. The consequences are such that it is standard recommended practice [Voigt 1928; Nye 1985] when using or measuring compliance values that the multiplying factor (ϕ) is always included in the reported value (*e.g.* it is implicit $S_{44} = 4S_{44}$). All compliance values reported in the present study follow this practice. [N.B. Wooster's [1949] treatment does not include multiplying factors of 2 or 4 in his reported S values. They must be applied later.]

2.4. Effects of Crystal Symmetry on *C* and *S* Matrices.

The number of independent coefficients in the 6 x 6 matrix array is reduced from 36 to 21 by a centre of symmetry (*e.g.* $C_{12} = C_{21}$, $C_{13} = C_{31}$ ….; $S_{12} = S_{21}$, $S_{13} = S_{31}$…, *etc.*) as evident in Eq. (7), and is further reduced by other symmetry elements such as axes of rotation, mirror planes and inversion such that some constants are zero and

others have equal values. The resulting effect for hexagonal crystal structures of all classes is to reduce the number of independent elastic constants to six [Voigt, 1928; Nye, 1985; Hearmon, 1979], as shown in the symmetrical 6 x 6 matrices in Eq. (8):

$$\begin{bmatrix}\sigma_1\\ \sigma_2\\ \sigma_3\\ \sigma_4\\ \sigma_5\\ \sigma_6\end{bmatrix}=\begin{bmatrix}C_{11} & C_{12} & C_{13} & \bullet & \bullet & \bullet\\ C_{12} & C_{11} & C_{13} & \bullet & \bullet & \bullet\\ C_{13} & C_{13} & C_{33} & \bullet & \bullet & \bullet\\ \bullet & \bullet & \bullet & C_{44} & \bullet & \bullet\\ \bullet & \bullet & \bullet & \bullet & C_{44} & \bullet\\ \bullet & \bullet & \bullet & \bullet & \bullet & C_{66}\end{bmatrix}\begin{bmatrix}\varepsilon_1\\ \varepsilon_2\\ \varepsilon_3\\ \gamma_4\\ \gamma_5\\ \gamma_6\end{bmatrix}\qquad \begin{bmatrix}\varepsilon_1\\ \varepsilon_2\\ \varepsilon_3\\ \gamma_4\\ \gamma_5\\ \gamma_6\end{bmatrix}=\begin{bmatrix}S_{11} & S_{12} & S_{13} & \bullet & \bullet & \bullet\\ S_{12} & S_{11} & S_{13} & \bullet & \bullet & \bullet\\ S_{13} & S_{13} & S_{33} & \bullet & \bullet & \bullet\\ \bullet & \bullet & \bullet & S_{44} & \bullet & \bullet\\ \bullet & \bullet & \bullet & \bullet & S_{44} & \bullet\\ \bullet & \bullet & \bullet & \bullet & \bullet & S_{66}\end{bmatrix}\begin{bmatrix}\sigma_1\\ \sigma_2\\ \sigma_3\\ \sigma_4\\ \sigma_5\\ \sigma_6\end{bmatrix} \tag{8}$$

$$C_{66}=(C_{11}-C_{12})/2 \qquad S_{66}=2(S_{11}-S_{12})$$

The 6 x 6 matrices in Eq. (8) are related to each other via matrix inversion. Consequently if the compliances (S_{mn}) are known then the corresponding stiffness constants (C_{mn}) may be obtained via matrix inversion and *vice versa*. This is important because initial compliance measurements were most easily measured via static techniques such as bending and torsion tests [Hearmon, 1946] whereas stiffness may not be measured in this manner (*e.g.* it is difficult to conduct a static tensile test for a uniaxial strain situation because three orthogonal stresses are necessary). However, experiments involving propagation of longitudinal and transverse elastic waves allow measurement of the C_{mn} because the tensile stiffness in a specific direction is related to the density of the test material and the velocity of the longitudinal wave in the same direction [Rowland and White, 1972; Gebrande, 1982; Blessing, 1990; Lim *et al.* 2001]. Similarly, the shear stiffness on a specific plane is related to the velocity of the shear wave on that plane and the density of the test material.

3. METAL HCP CRYSTALS

3.1. Crystallography.

The crystallographic nature of the hexagonal metal structures is shown in Fig. 3. The unit cell in (a) has two axes a_1 and a_2 of equal length inclined at 60°, and an orthogonal axis of different length c. Fig. 3(b) shows the principal crystallographic directions in the (0001) basal plane expressed in the Miller-Bravais system [Cullity, 1956] using four axes composed of three planar a-axes ($a_1 = a_2 = a_3$) at 120° to each other and the orthogonal c-axis. Fig 3(c) shows the relationship between the orthogonal X-axes in Fig. 1 and crystallographic directions.

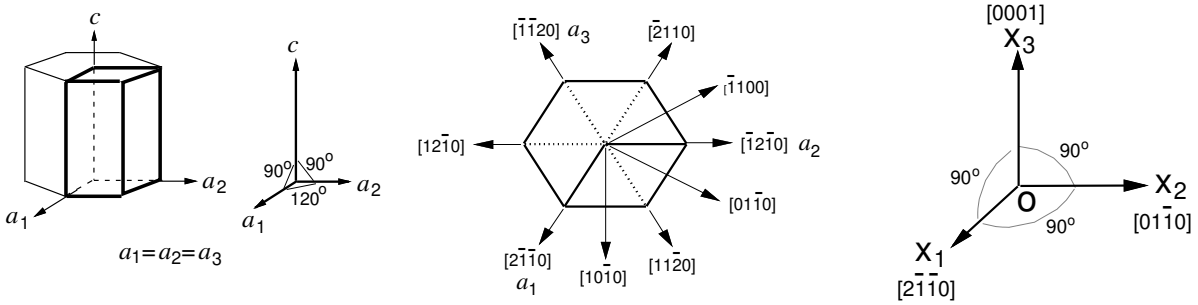

Figure 3 HCP metal crystallography.(a) Unit cell showing the a_1, a_2, and c-axes. (b) Directions in Miller-Bravais indices. (c) Relationship between X_1, X_2 and X_3 axes in Figure 1 and crystallographic directions.

When defining and measuring compliance and stiffness constants it is most important that the orthogonal axes X_1 X_2 and X_3 in Fig.1 conform to standardised orthogonal directions in the HCP crystals (Nye). These directions are shown in Fig 3(c) where $X_1 = [2\bar{1}\bar{1}0]$ *i.e.* the a_1-axis, $X_2 = [01\bar{1}0]$ and $X_3 = [0001]$ *i.e.* the c-axis. All S and C constants are reported with respect to these axial directions. For example in Fig.1, σ_{33} and ε_{33} correspond to tensile stresses and strains in the [0001] direction and S_{33} and C_{33} correspond to the compliance and stiffness constants, respectively, measured in the [0001] direction.

3.2. HCP Metals Examined.

Twenty four hexagonal structured metals with an atomic number (At. No.) ranging from 4 to 81were examined. All belong to the crystal class $P6_3/mmc$. They are listed in Table 1 in order of their At. No., together with their *c/a* ratio and density (ρ) obtained from Metals Handbook [1985]. The ideal *c/a* ratio required for close packing of spheres to form the HCP structure is 1.633 (*i.e.* $\sqrt{24}/3$).

Table 1. Hexagonal crystals studied with c/a ratio and density ρ.

At. No.	Metal	*c/a*	ρ (g cm^{-3})	At. No.	Metal	*c/a*	ρ (g cm^{-3})
4	Be α-Beryllium	1.56803	1.85	60	Nd α-Neodymium‡	3.22404	7.00
12	Mg Magnesium	1.62350	1.74	64	Gd α-Gadolinium	1.58791	7.86
21	Sc α-Scandium	1.59215	2.9	65	Tb α-Terbium	1.58056	8.25
22	Ti α-Titanium	1.58734	4.51	66	Dy α-Dysprosium	1.57382	8.55
27	Co α-Cobalt	1.62283	8.85	67	Ho α-Holmium	1.56983	8.79
30	Zn Zinc	1.85635	7.13	68	Er α-Erbium	1.52877	9.15
39	Y α-Yttrium	1.56986	4.47	69	Tm α-Thulium	1.57932	9.31
40	Zr α-Zirconium	1.59312	6.49	71	Lu α-Lutetium	1.57143	9.85
44	Ru Ruthenium	1.58330	12.45	72	Hf α-Hafnium	1.58147	13.1
48	Cd Cadmium	1.88572	8.65	75	Re Rhenium	1.61522	21.0
57	La α-Lanthanum‡	3.22546	6.15	76	Os Osmium	1.57993	22.61
59	Pr α-Praseodymium‡	3.22616	6.77	81	Tl α-Thallium	1.59821	11.85

Three metals La, Pr and Nd have the DHCP (double HCP) structure where the stacking of close packed planes follows the order ABACABAC instead of the usual HCP sequence ABAB [Nareth, 1969]. Consequently, close packing under these conditions leads to an ideal c/a ratio of 3.3256. Overall, most of the metals were lower and within -0.1 of their ideal c/a ratio, except for Cd and Zn which exceeded the ratio by 0.223 and 0.194, respectively.

Values for the five independent stiffness and compliance constants of all twenty four hexagonal metals were obtained from the published literature and listed in Table 2. Most were obtained from the data compiled by Hearmon [1979]. Additionally, as noted at the foot of Table 2, constants for the metals La, Os, Tm and Tl were obtained from (a) Ouyang *et al.* [2009], (b) Pantea *et al*. [2008], (c)Lim *et al*. [2001] and Singh [1999], and (d) the combined averages of Ferris *et al*. [1963] and Weil and Lawson [1966]. A matrix inversion of *C* to *S*, and vice versa (see Eq. (8)), was conducted by the author to confirm consistency between the stiffness and compliance values. In some instances only *C*-values were measured and reported, in which case the author used matrix inversion to obtain the corresponding *S*-values. In the case of La no experimental measurements were available, possibly due to the difficulty of growing single crystals of the DHCP α-phase which were free from the metastable FCC β-phase phase at room temperature [Stassis *et al*.1982, Dixon *et al*. 2008]. Consequently, the theoretical stiffness calculations of La by Ouyang et al [2009] were employed because their work shows reasonable correlation between measured and theoretical values in other hexagonal metal crystals.

Table 2. Stiffness and Compliance Data. Hearmon [1979], unless indicated otherwise.

Metal	Stiffness Constants (GPa)					Compliance Constants (TPa)$^{-1}$				
	C_{11}	C_{33}	C_{44}	C_{12}	C_{13}	S_{11}	S_{33}	S_{44}	S_{12}	S_{13}
Be	292	349	163	24	6	3.45	2.87	6.14	-0.28	-0.05
Mg	59.3	61.5	16.4	25.7	21.4	22.0	19.7	60.98	-7.75	-4.96
Sc	99.3	107	27.7	39.7	29.4	12.46	10.57	36.1	-4.32	-2.24
Ti	160	181	46.5	90	66	9.62	6.84	21.5	-4.67	-1.81
Co	295	335	71	159	111	4.99	3.56	14.08	-2.36	-0.87
Zn	165	61.8	39.6	31.1	50	8.07	27.55	25.25	0.606	-7.02
Y	77.9	76.9	24.3	29.2	20	15.44	14.4	41.15	-5.10	-2.69
Zr	144	166	33.4	74	67	10.20	8.01	29.94	-4.09	-2.46
Ru	563	624	181	188	168	2.09	1.82	5.525	-0.576	-0.408
Cd	116	50.9	19.6	43	41	12.20	33.76	51.02	-1.32	-8.763
La[(a)]	51.44	54.63	13.92	17.27	10.4	22.35	19.42	71.84	-6.91	-2.94
Pr	49.4	57.4	13.6	23	14.3	26.60	19.32	73.53	-11.28	-3.82
Nd	54.8	60.9	15.0	24.6	16.6	23.66	18.53	66.66	-9.45	-3.87
Gd	67.25	71.55	20.75	25.3	21	18.15	16.12	48.19	-5.686	-3.659
Tb	68.55	73.3	21.6	24.65	22.4	17.68	16.0	46.30	-5.10	-3.84
Dy	74	78.6	34.3	25.5	21.8	16.03	14.48	41.15	-4.59	-3.17
Ho	76.5	79.6	25.9	25.6	21	15.32	14.1	38.60	-4.33	-2.90
Er	84.1	84.7	27.4	29.4	22.6	14.10	13.2	36.50	-4.21	-2.63
Tm[(c)]	92.5	81.5	28.2	33.5	21	12.82	13.42	35.46	-4.133	-2.237
Lu	86.2	80.9	26.8	32	28	14.28	14.79	37.30	-4.17	-3.50
Hf	181	197	55.7	77	66	7.15	6.13	18.0	-2.47	-1.57
Re	616	683	161	273	206	2.11	1.70	6.210	-0.804	-0.394
Os[(b)]	765	846	270	229	219	1.501	1.334	3.704	-0.365	-0.294
Tl[(d)]	41.35	53.85	7.23	36	29.45	104.5	31.80	138.3	-82.40	-12.12

(*a) Ouyang et al. [2009]: (b) Pantea et al. [2008], (c) Lim et al. [2001] except C_{13} which is the average of the interpolated value of 25 GPa by Lim et al. [2008] and a calculated value of ~17 GPa by Singh [1999]: (d) Average of data from Ferris et al [1963] and Weil and Lawson [1966].*

3.3 Stiffness.

The most important aspect of uniaxial strain conditions is the three dimensional stress state where the presence of lateral tensile stresses allows no lateral strain contractions *i.e*. Poisson's ratio is zero. This is readily evident from an examination of the stiffness (*C*) relationships in Eq. (8), leading to Eq. (9), for uniaxial strains ε_1, ε_2 and ε_3 :

$$\begin{aligned}
&\varepsilon_1 : (\varepsilon_2 = \varepsilon_3 = 0): \quad \sigma_1 = C_{11}\varepsilon_{11},\ \sigma_2 = C_{12}\varepsilon_1,\ \sigma_3 = C_{13}\varepsilon_1 \\
&\varepsilon_2 : (\varepsilon_1 = \varepsilon_3 = 0): \quad \sigma_2 = C_{11}\varepsilon_2,\ \sigma_1 = C_{12}\varepsilon_2,\ \sigma_3 = C_{13}\varepsilon_2 \\
&\varepsilon_3 : (\varepsilon_1 = \varepsilon_2 = 0): \quad \sigma_3 = C_{33}\varepsilon_3,\ \sigma_1 = C_{13}\varepsilon_3,\ \sigma_2 = C_{13}\varepsilon_3
\end{aligned} \tag{9}$$

3.4 Young's Modulus *E* and Rigidity (Shear) Modulus *G*.

The tensile modulus *E* is the constant of proportionality between stress and strain under uniaxial stress loading as measured in the direction of the applied stress (*i.e.* a three dimensional strain situation). It has wide application in engineering design. Examination of the compliance (*S*) relationships in Eq. (8) under a uniaxial stress σ_1, σ_2 or σ_3 yields the relationships shown in Eq. (10) where it is evident that *E* is the reciprocal compliance S^{-1}:

$$\begin{aligned}
&\sigma_1 : (\sigma_2 = \sigma_3 = 0): \quad E_{(2\bar{1}\bar{1}0)} = \sigma_1/\varepsilon_1 = (S_{11})^{-1} \quad \varepsilon_2 = S_{12}\sigma_1,\ \varepsilon_3 = S_{13}\sigma_1 \\
&\sigma_2 : (\sigma_1 = \sigma_3 = 0): \quad E_{(01\bar{1}0)} = \sigma_2/\varepsilon_2 = (S_{11})^{-1} \quad \varepsilon_1 = S_{12}\sigma_2,\ \varepsilon_3 = S_{13}\sigma_2 \\
&\sigma_3 : (\sigma_1 = \sigma_2 = 0): \quad E_{(0001)} = \sigma_3/\varepsilon_3 = (S_{33})^{-1} \quad \varepsilon_1 = S_{13}\sigma_3,\ \varepsilon_2 = S_{13}\sigma_3
\end{aligned} \tag{10}$$

The subscripts $(2\bar{1}\bar{1}0)$, $(01\bar{1}0)$ and (0001) in Eq. [10] refer to the crystal plane lying normal to the direction of the uniaxial stress (see Figs. 3 and 4) and the corresponding *E* values are listed in Table 3.

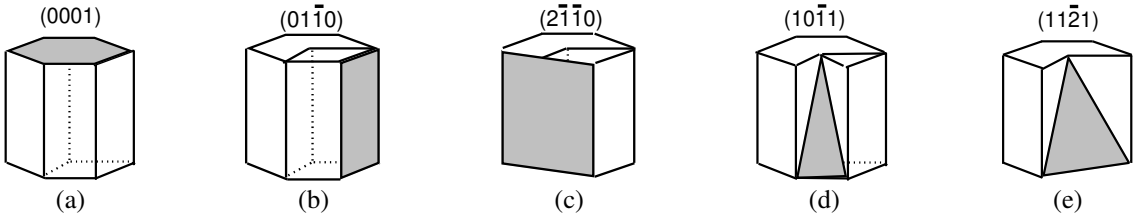

Figure 4. Orientations and Miller-Bravais indices of principal planes in hexagonal crystals (a) basal plane, (b) primary prismatic plane: (c) secondary prismatic plane: (d) primary pyramidal plane and (e) secondary pyramidal plane.

For uniaxial stresses σ_1, σ_2, and σ_3 the corresponding average Poisson's ratios, ν_1 ν_2 and ν_3 are obtained:

$$\nu_1 = \frac{-(\varepsilon_2+\varepsilon_3)}{2\varepsilon_1} = \frac{-(S_{12}+S_{13})}{2S_{11}};\quad \nu_2 = \frac{-(\varepsilon_1+\varepsilon_3)}{2\varepsilon_2} = \frac{-(S_{12}+S_{13})}{2S_{11}};\quad \nu_3 = \frac{-(\varepsilon_2+\varepsilon_1)}{2\varepsilon_3} = \frac{-(S_{13}+S_{13})}{2S_{33}}; \tag{11}$$

The negative sign in the formulae for Poisson's ratio in Eq. (11) is introduced because the lateral strains are usually contractions (negative strain) and it is conventional to express ν as a positive number. Note that the ratios of the two components S_{12}/S_{11} and S_{13}/S_{11} in ν_1 and ν_2 are unequal leading to different lateral strains in orthogonal directions X_1 and X_3 in the $(2\bar{1}\bar{1}0)$ prismatic plane and orthogonal directions X_2 and X_3 in the $(01\bar{1}0)$ prismatic plane (see Figs. 3 and 4). Zinc is an unusual metal because S_{12} has a positive value (see Table 2) indicating that there is an expansion along the c-axis in the X_3 direction on the prismatic planes (i.e. a negative ν of $-S_{12}/S_{11}$ = -0.075 in the X_3 direction). Similar negative ν-values on prismatic planes of Zn have been reported previously [Lubarda and Meyers, 1999] Although uncommon, negative ν-values are not forbidden by thermodynamics and have been reported for several metal crystals of cubic symmetry when stretched in the [110] direction [Baughman *et al*., 1998] and in the mineral cristobalite [Yeganeh-Haeri *et al*. 1992]. Based on Eq. (11) average values of Poisson's ratio ν_1 and ν_2 on the prismatic planes, and ν_3 on the basal plane, are listed in Table 3.

Conditions of pure shear are produced under torsional loading where the stresses involved are readily seen by an examination of Figs. 1, 3 and 4. If torsion is produced on the $(2\bar{1}\bar{1}0)$ prismatic plane by rotation around the X_1 axis the shear stresses involved are σ_{31} and σ_{21} (*i.e*. σ_5 and σ_6 in the contracted notation). Similarly, torsion produced on

the $(01\bar{1}0)$ prismatic plane by rotation around the X_2 axis involves the shear stresses σ_{32} and σ_{12} (*i.e.* σ_4 and σ_6), whereas torsion on the (0001) basal plane via rotation around the X_3 axis requires the shear stresses σ_{13} and σ_{23} (i.e. σ_4 and σ_5). Consequently, from Eq.(12), the average shear compliances S_G on the $(2\bar{1}\bar{1}0)$, $(01\bar{1}0)$ and (0001) planes are obtained:

$$S_{G(2\bar{1}\bar{1}0)} = \left[\frac{\varepsilon_5/\sigma_5 + \varepsilon_6/\sigma_6}{2}\right] = \left[\frac{S_{55}+S_{66}}{2}\right] = \left[\frac{S_{44}+2S_{11}-2S_{12}}{2}\right]$$
$$S_{G(01\bar{1}0)} = \left[\frac{\varepsilon_4/\sigma_4 + \varepsilon_6/\sigma_6}{2}\right] = \left[\frac{S_{44}+S_{66}}{2}\right] = \left[\frac{S_{44}+2S_{11}-2S_{12}}{2}\right] \quad (12)$$
$$S_{G(0001)} = \left[\frac{\varepsilon_4/\sigma_4 + \varepsilon_5/\sigma_5}{2}\right] = \left[\frac{S_{44}+S_{55}}{2}\right] = S_{44}$$

Hence, the shear modulus G on each crystal plane is simply the reciprocal compliance $(S_G)^{-1}$ and is listed in Table 3 for the different hexagonal metal crystals.

Table 3. Young's Modus (E), Poisson's Ratio ν, and Shear Modulus (G)

Metal	$E_{(2\bar{1}\bar{1}0)}, E_{(01\bar{1}0)}$ (GPa)	$E_{(0001)}$ (GPa)	$(\nu_1)_{(2\bar{1}\bar{1}0)}, (\nu_2)_{(01\bar{1}0)}$	$(\nu_3)_{(0001)}$	$G_{(2\bar{1}\bar{1}0)}, G_{(01\bar{1}0)}$ (GPa)	$G_{(0001)}$ (GPa)
Be	290	348.4	0.0479	0.0174	147.1	162.3
Mg	45.5	50.76	0.289	0.252	16.6	16.4
Sc	80.3	94.67	0.263	0.212	28.7	27.7
Ti	104	146.2	0.337	0.265	39.9	46.5
Co	200	280.9	0.324	0.244	69.5	71.0
Zn	124	36.3	0.397	0.255	49.8	39.6
Y	64.8	69.44	0.252	0.187	24.3	24.3
Zr	98	124.8	0.321	0.307	34.2	33.4
Ru	478	549.5	0.235	0.224	184.2	181
Cd	82	29.62	0.413	0.259	25.6	19.6
La[a]	44.7	51.49	0.220	0.151	15.3	13.9
Pr	37.6	51.76	0.284	0.198	13.4	13.6
Nd	42.3	53.97	0.281	0.209	15.1	15.0
Gd	55.1	62.04	0.257	0.227	20.9	20.8
Tb	56.6	62.5	0.253	0.240	21.8	21.6
Dy	62.4	69.06	0.242	0.219	24.3	24.3
Ho	65.3	70.92	0.236	0.206	25.7	25.9
Er	70.9	75.76	0.243	0.199	27.4	27.4
Tm[c]	78	74.5	0.248	0.167	28.8	28.2
Lu	70	67.6	0.269	0.237	27.0	26.8
Hf	140	163.1	0.283	0.256	53.7	55.6
Re	474	588.2	0.284	0.232	166	161
Os[b]	666	749.6	0.220	0.220	269	270
Tl[d]	9.57	31.45	0.452	0.381	3.91	7.23

3.5 Representation of Angular Anisotropy of *E* and *G*.

While the magnitude and anisotropy of the elastic moduli is indicated in Table 3 for the three principal planes, it is desirable to know the full effect of differently oriented planes on the values of *E* and *G* in hexagonal crystals. For example, consider a plane which makes intercepts *x*, *y* and *z* on the X_1 X_2 and X_3 axes, respectively, as shown in Fig. (5a). Let the direction of the normal (N) to this plane make an angel θ with respect to the X_3 axis. The X_1 X_2 and X_3 axes are now rotated to the positions X_1', X_2' and X_3' while remaining orthogonal so that the angle between X_3 and X_3' is θ, as shown in Fig. 5(b). It is evident from Eq. (10) that the tensile compliance on the *xyz* plane is S_{33}' with a corresponding tensile modulus $E_\theta = (S_{33}')^{-1}$. Similarly, from Eq. (12), the shear compliance on the same plane is $S_G' = (S_{44}' + S_{55}')/2$ and $G_\theta = (S_G')^{-1}$, where S_{33}', S_{44}' and S_{55}' are calculated with respect to the new (transformed) axes X_1', X_2' and X_3'. [N.B. While $S_{44} = S_{55}$ when using the standard X_1 X_2 and X_3 axes as shown in Eq. (12),

$S'_{44} \neq S'_{55}$ when referred to the transformed axes [Voigt 1928]. Furthermore, transformation of compliances to the new axes must be conducted in the full tensor notation (see Eq. (5)) after which values may be converted to the contracted matrix notation [Nye 1985]. Transformation is a tedious procedure aided by the resulting cylindrical symmetry of the compliances with respect to the *c*-axis of the unit cell. Calculations of the transformed compliances were first conducted by Voigt [1928, pg. 746-747] to yield Eqs. (13) and (14):

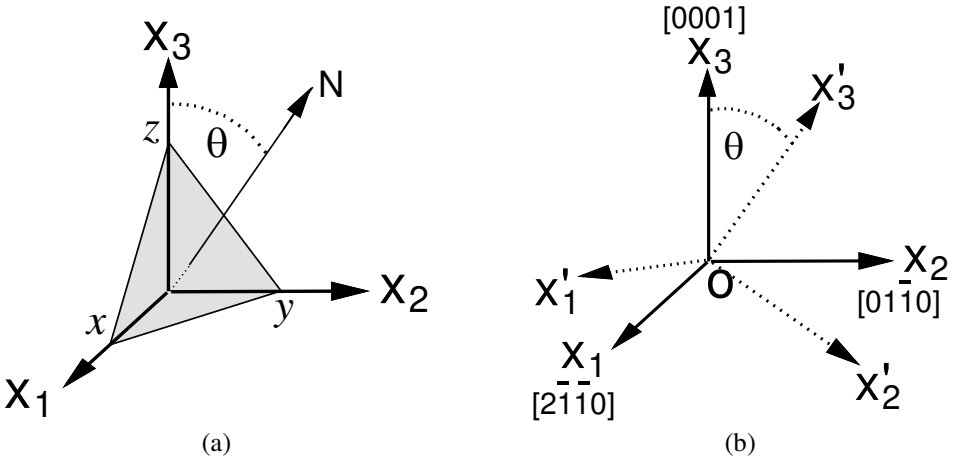

Figure 5. (a) Direction (θ degrees) of the normal N to the plane xyz with respect to X_3 *(b) Transformed orthogonal axes* X'_1, X'_2 *and* X'_3 *such that* X'_3 *is rotated by* θ *to coincide with N direction.*

$$S'_{33} = S_{11}(\sin^4\theta) + S_{33}(\cos^4\theta) + (2S_{13} + S_{44})(\cos^2\theta)(\sin^2\theta) \tag{13}$$

$$S'_G = (S'_{44} + S'_{55})/2 = S_{44} + (S_{11} - S_{12} - 0.5S_{44})(\sin^2\theta) + 2(S_{11} + S_{33} - 2S_{13} - S_{44})(\cos^2\theta\sin^2\theta) \tag{14}$$

Voigt's [1928] original equations were written in terms of $\cos^2\theta$ and $(1-\cos^2\theta)$. In Eqs. (13) and (14) the original $(1-\cos^2\theta)$ terms have been replaced by $\sin^2\theta$. Note that when θ equals 0^o and 90^o, Eq. (13) shows that $(S'_{33})^{-1}$ is equivalent to $(S_{33})^{-1}$ and $(S_{11})^{-1}$, respectively, consistent with Eq. (10). Similarly, in regard to Eq. (14), S'_G is equivalent to S_{44} when $\theta = 0^o$, and S'_G is equivalent to $(S_{44} + 2S_{11} - 2S_{12})/2$ when $\theta = 90^o$, consistent with Eq. (12).

Based on Eqs. (13) and (14), together with the relationships $E_\theta = (S'_{33})^{-1}$ and $G_\theta = (S'_G)^{-1}$ the angular variations of Young's modulus (E) and the shear modulus (G)for all metals listed in Table 1 may be represented graphically, via θ *versus E* and θ *versus G* diagrams . This is shown for the three metals Zn, Mg and Cd in Fig. 6 where the main consideration determining the combination was a reasonable similarity in magnitude between the *E* moduli and *G* moduli of each metal. It is readily evident that Zn and Cd are markedly anisotropic in behaviour, particularly Zn, whereas Mg tends to be considerably less anisotropic. Furthermore, the cylindrical symmetry of the behaviours of *E* and *G* with respect to the X_3 axis (*i.e.* c-axis, [0001] direction) is evident in Fig 6, and evident in subsequent Figs. 7 and 8, via the mirror image of the angular data on either side of the X_3 axis.

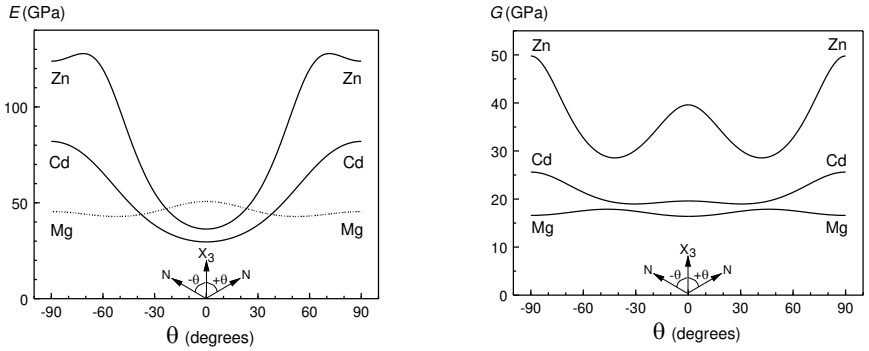

Figure 6. Angular variation of E and G for Zn, Cd and Mg

The other twenty one metals investigated were also grouped in figures where there was a reasonable similarity in the magnitudes of the moduli. Thus, Fig. 7 shows the angular modulus behaviours of E and G for $0^o < \theta < 90$ for three groups of metals: Hf, Ti, Zr, Sc, and Y; Tm; Lu, Ho, Tb, and La; Er, Dy, Gd, Nd, Pr and Tl.

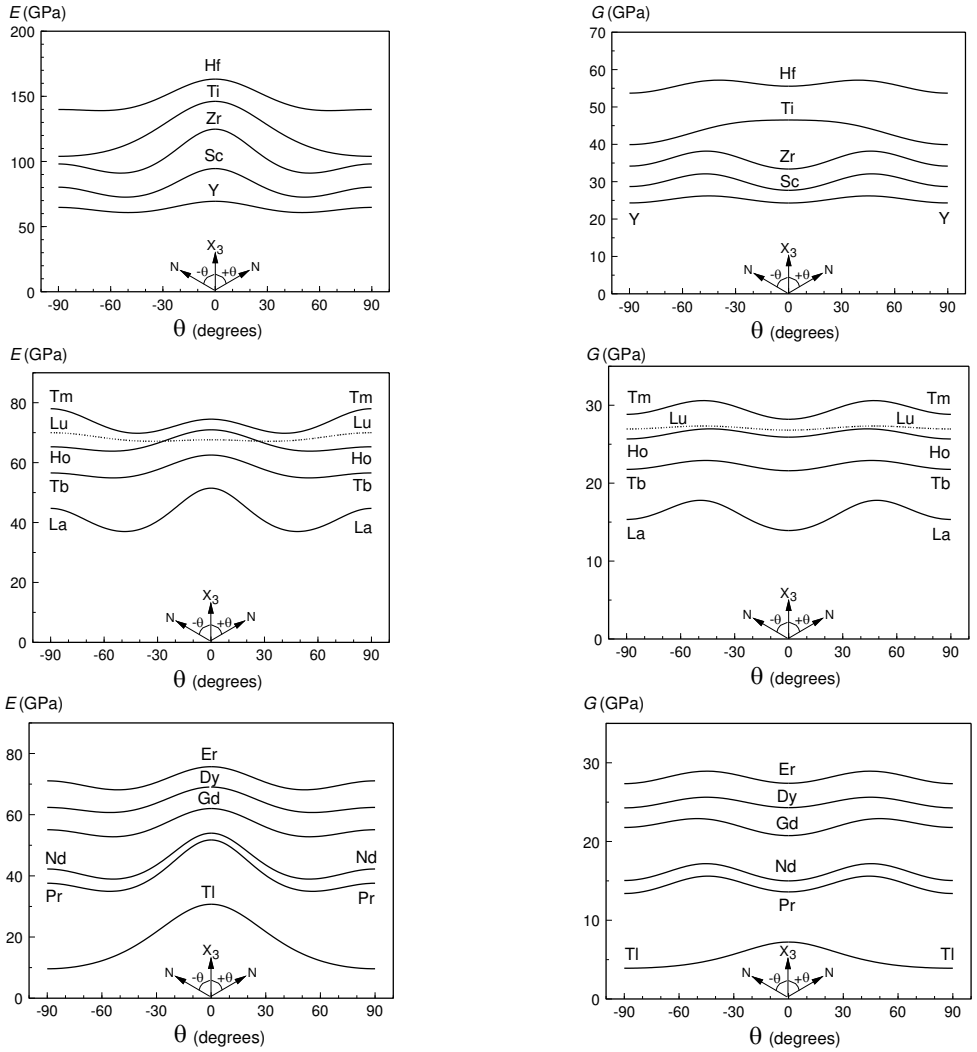

Figure 7. Angular variation of E and G for Hf, Ti, Zr, Sc and Y: Tm, Lu, Ho, Tb and La: Er, Dy Gd Nd Pr and La.

As a general observation, with the exception Ti and Tl, E-behaviour in Fig 7 tends to exhibit a maximum on the (0001) basal plane (*i.e*. when θ is zero and N coincides with the [0001] direction) and a maximum (in most cases) on the prismatic planes where θ is 90^o. Additionally, in most cases, E tends to exhibit a minimum value between $0^o < \theta < 90^o$. In contrast, G tends to exhibit a minimum when θ is zero and 90^o, and a maximum for $0^o < \theta < 90^o$. In the case of Ti and Tl, the behaviours of E and G are similar, exhibiting a maximum when θ is zero and a minimum when θ is 90^o.

The group Os, Ru, Re, Be and Co exhibit the highest moduli of all the HCP metals and their collective behaviour is shown in Fig. 8. All show a pronounced maximum value of E on the basal plane, for which θ is zero, and a tendency by Ru, Re and Co to exhibit a minimum between $0^o < \theta < 90$. With the exception of Be, the G-behaviour exhibits a minimum when θ is zero and 90^o, and a maximum for $0^o < \theta < 90^o$. In the case of Be, a maximum G occurs when θ is zero, indicating G is highest on the basal plane. Overall, Figs 6 to 8 demonstrate a remarkably wide difference in the maximum E values in HCP metal crystals, ranging from an extremely high value of 749.6 GPa for Os (Fig. 8) to a low of 32.5 GPa for Tl (Fig. 7).

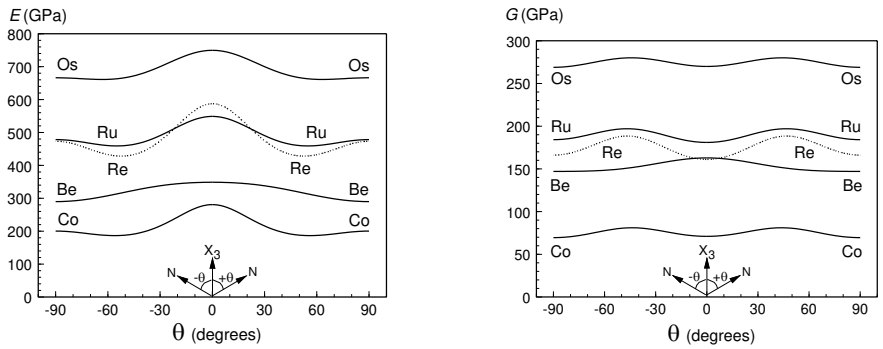

Figure 8. Angular variation of E and G for Os, Ru, Re, Be and Co

The presence and precise position of an intermediate maximum or minimum E at $0 < \theta < 90$ degrees in most of the graphical plots in Figs 6 to 8, due to a minimum or maximum in S'_{33}, was ascertained by differentiating Eq. (13) and placing the first differential equal to zero:

$$\partial S'_{33}/\partial\theta = 4S_{11}\sin^3\theta\cos\theta - 4S_{33}\cos^3\theta\sin\theta + 2(2S_{13}+S_{44})(\sin\theta\cos^3\theta - \cos\theta\sin^3\theta) = 0 \quad (15)$$

$$\text{with solutions } \theta = 0^o,\ \theta = 90^o, \text{ and } \tan\theta = [(S_{44}+2S_{13}-2S_{33})/(S_{44}+2S_{13}-2S_{11})]^{1/2}$$

Similar procedures were applied to calculate the position of intermediate maxima/minima for G at $0< \theta <90$ degrees in Figs 6 to 8, due to a minimum or maximum in S'_G, by placing the first differential of Eq. (14) equal to zero:

$$\partial S'_G/\partial\theta = (2S_{11}-2S_{12}-S_{44})\cos\theta\sin\theta + 4(S_{11}+S_{33}-S_{44}-2S_{13})(\sin\theta\cos^3\theta - \cos\theta\sin^3\theta) = 0 \quad (16)$$

$$\text{with solutions } \theta = 0,\ \theta = 90^o, \text{ and } \cos 2\theta = [(S_{44}+2S_{12}-2S_{11})/4(S_{11}+S_{33}-S_{44}-2S_{13}]$$

The E and G values at 0^o and 90^o are already listed under the respective basal plane heading (0001) and prismatic plane headings $(2\bar{1}\bar{1}0)$, and $(01\bar{1}0)$ in Table 3. The calculated intermediate max/min values of E and G and their corresponding angles θ in degrees, based on Eqs. (15) and (16), are listed in Table 4.

Table 4. Calculated modulus and θ values at intermediate peak max/min for HCP crystals.

Metal	θ°	*E* (GPa)	θ°	*G* (GPa)	Metal	θ°	*E* (GPa)	θ°	*G* (GPa)
Be	●	●	●	●	Nd	53.93	38.95 (min)	45.19	17.19 (max)
Mg	52.11	42.85 (min)	46.13	17.88 (max)	Gd	53.95	52.79 (min)	45.56	22.34 (max)
Sc	51.36	72.63 (min)	47.12	32.11 (max)	Tb	54.94	54.90 (min)	46.07	22.91 (max)
Ti	●	●	●	●	Dy	55.56	60.72 (min)	44.85	25.63 (max)
Co	56.08	186.62 (min)	43.83	81.06 (max)	Ho	55.58	63.83 (min)	43.52	26.97 (max)
Zn	71.47	127.81 (max)	41.97	28.56 (min)	Er	51.60	68.14 (min)	44.78	28.94 (max)
Y	50.05	60.80 (min)	45.08	26.20 (max)	Tm	41.37	69.81 (min)	47.35	30.60 (max)
Zr	54.38	91.08 (min)	46.43	38.19 (max)	Lu	32.75	67.14 (min)	47.33	27.34 (max)
Ru	54.88	459.12 (min)	46.73	197.01 (max)	Hf	65.10	139.06 (min)	39.34	57.18 (max)
Cd	●	●	30.62	18.98 (min)	Re	52.37	428.26 (min)	46.70	188.48 (max)
La	48.48	37.01 (min)	48.96	17.80 (max)	Os	63.23	661.13 (min)	44.28	280.08 (max)
Pr	55.69	34.94 (min)	44.20	15.60 (max)	Tl	●	●	●	●

Based on the *c/a* ratio, the angle θ between the (0001) plane and an arbitrary plane (*hkil*) in the hexagonal system is given by Eq. (17) [Cullity, 1956]; with results for several planes listed in Table 5.

$$\cos\theta = 0.75(a/c)^2 l\{0.75(a/c)^2(h^2+k^2+hk+0.75(a/c)^2 l^2)\}^{-1/2} \quad (17)$$

Table 5. Calculate angles between the (0001) and selected (hkil) planes.

Metal HCP	c/a Ratio	$(10\bar{1}1)$	$(11\bar{2}1)$	$(10\bar{1}2)$	$(11\bar{2}2)$	$(10\bar{1}3)$	$(20\bar{2}3)$
		θ degrees	θ degrees	θ degrees	θ degrees	θ degrees	θ degrees
Be	1.56803	61.09	72.31	42.15	57.47	31.11	50.36
Mg	1.6235	61.92	72.88	43.15	58.37	32.00	51.34
Sc	1.59215	61.46	72.57	42.59	57.87	31.50	50.79
Ti	1.58734	61.38	72.52	42.50	57.79	31.42	50.70
Co	1.62283	61.91	72.88	43.14	58.36	31.99	51.32
Zn	1.85635	64.99	74.93	46.98	61.69	35.55	55.02
Y	1.56986	61.12	72.33	42.19	57.50	31.14	50.39
Zr	1.59312	61.47	72.58	42.61	57.88	31.52	50.81
Ru	1.5833	61.32	72.47	42.43	57.72	31.36	50.63
Cd	1.88572	65.33	75.15	47.43	62.06	35.97	55.44
Gd	1.58791	61.39	72.52	42.51	57.80	31.43	50.71
Tb	1.58056	61.28	72.45	42.38	57.68	31.31	50.58
Dy	1.57382	61.18	72.38	42.26	57.57	31.21	50.46
Ho	1.56983	61.12	72.33	42.19	57.50	31.14	50.39
Er	1.52877	60.47	71.89	41.43	56.81	30.47	49.64
Tm	1.57932	61.26	72.43	42.36	57.66	31.29	50.56
Lu	1.57143	61.14	72.35	42.22	57.53	31.17	50.42
Hf	1.58147	61.29	72.46	42.40	57.69	31.33	50.60
Re	1.61522	61.80	72.80	43.00	58.24	31.87	51.19
Os	1.57993	61.27	72.44	42.37	57.67	31.30	50.57
Tl	1.59821	61.55	72.63	42.70	57.97	31.60	50.90
Metal DHCP	c/a Ratio	$(10\bar{1}2)$	$(11\bar{2}2)$	$(10\bar{1}4)$	$(11\bar{2}4)$	$(10\bar{1}6)$	$(20\bar{2}6)$
		θ degrees	θ degrees	θ degrees	θ degrees	θ degrees	θ degrees
La	3.22546	61.76	72.77	42.96	58.20	31.83	51.15
Pr	3.22616	61.77	72.78	42.96	58.20	31.84	51.15
Nd	3.22404	61.75	72.77	42.94	58.19	31.82	51.14

Examination of Tables 4 and 5 indicates that in most cases the intermediate minimum values of E for HCP structures occur on planes inclined at angles of ~50° to 60° with respect to the (0001) plane, corresponding to a mix of planes of the type $(20\bar{2}3)$, $(11\bar{2}2)$ and $(10\bar{1}1)$. In contrast, intermediate maximum values of G occur at angles of approximately 45° ±2° corresponding to planes of the type $(10\bar{1}2)$. In the case of the three DCHP metals La, Pr and Nd, the minimum values of E are between ~48° and ~56°, near 50°, corresponding to planes near $(20\bar{2}6)$ and the maximum G values occur at angles near 46° corresponding to planes near $(10\bar{1}4)$.

3.6 Polar Diagrams of *E* and *G*.

The θ *versus E* and θ *versus G* graphs are useful for comparing angular variations in moduli, but polar co-ordinate plots are more effective for assessing angular symmetry. Voigt [1928] and Wooster [1949] used compliance (S) polar plots for the mineral Beryl and Zinc. The present study uses polar plots of the modulus (*i.e.* reciprocal compliance S^{-1}) where E is treated as a vector with co-ordinates $E\sin\theta$ normal to the X_3 axis and co-ordinates $E\cos\theta$ parallel to the X_3 axis. The shear modulus G is treated in the same manner. Importantly, each vector (modulus) is normalized with respect to the modulus value at θ = 90° (*i.e.* $\sin\theta = 1$) so that metals having very different moduli may be compared in the same figure. If all crystals were perfectly symmetrical in their modulus behaviour all polar plots would be circles with a radius of unity. Deviations from circular behaviour readily indicate the degree and direction of anisotropic behaviour. as shown in Fig, 9 for Mg, Cd, Zn and Be, and Ti, Y, Co and Zr. Metal groupings in this and subsequent figures were chosen to minimise overlap of individual data sets.

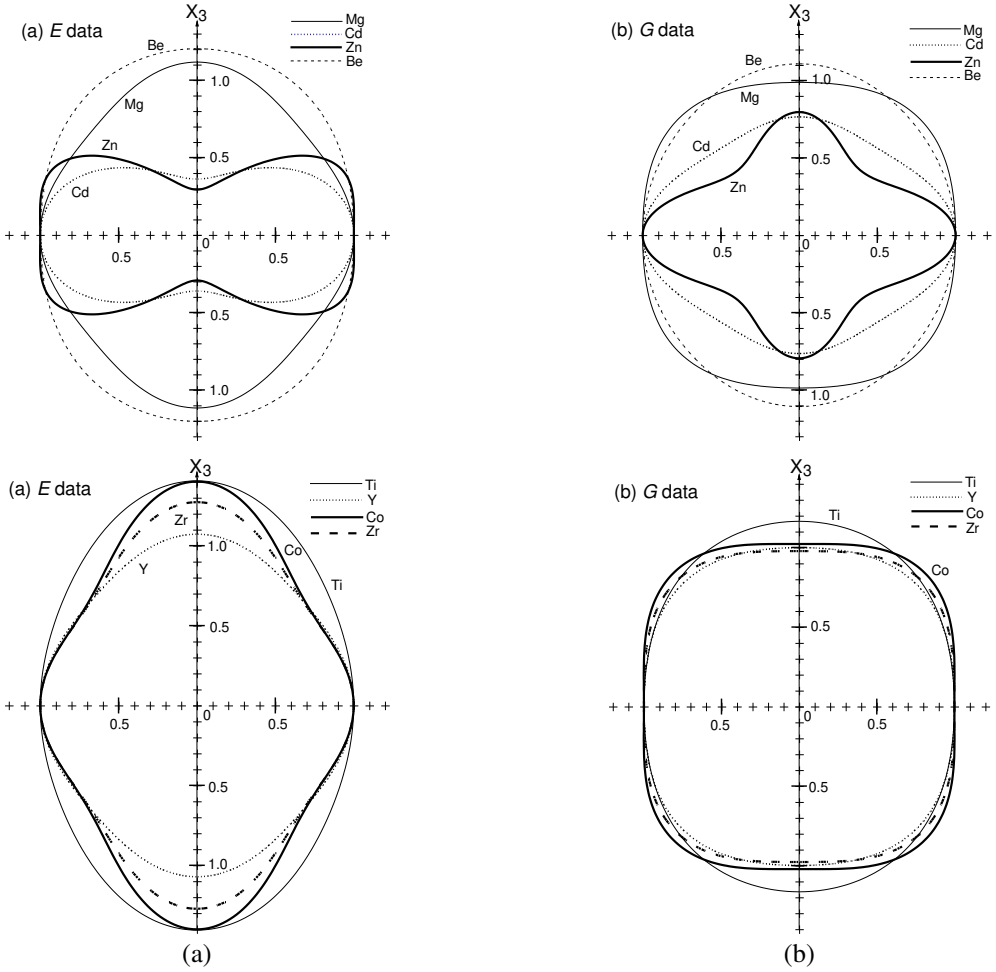

Figure 9. Normalized polar diagrams: Mg, Cd, Zn, Be (top) and Ti, Y, Co Zr (bottom). (a) E data: (b) G data.

It is evident that anisotropy in the normalized behaviour of Cd and Zn is extreme for both *E* and *G*, whereas Mg and Be approach a distorted circular symmetry. In the Ti, Y, Co and Zr group, Y exhibits the least anisotropy whereas Ti, Co and Zr have significant departures from circularity of *E* in the X_3 direction. The anisotropic behaviour of *G* behaviour is similar for Y, Co and Zr with Ti exhibiting a larger anisotropy in the X_3 direction.

Figure 10 shows the modulus behaviour of Nd, Sc, Lu and La, Re and Er. The approximate circular nature of the polar diagrams of *E* and *G* for Lu indicate it is almost isotropic in contrast to Nd and Sc which exhibit distorted circles in the X_3 direction. Regarding La, Re and Er, all three show distorted circular symmetry in their *E*-behaviour. However, in the case of their *G*-behaviour, Er approaches circular symmetry more closely.

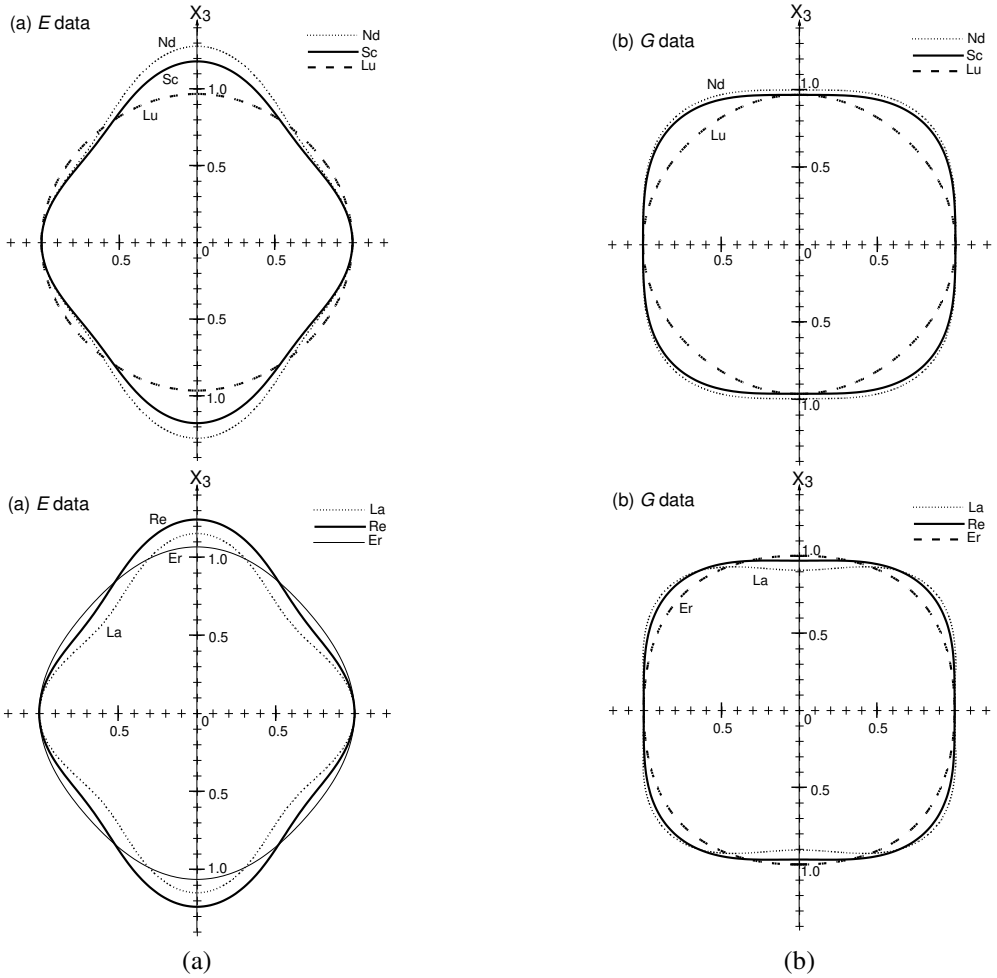

Figure 10. Normalized polar diagrams: Nd, Sc, Lu, (top) and La, Re Er (bottom). (a) E data: (b) G data.

Extreme departure from circularity (X_3 extension) in the modulus behaviour of Tl is shown in Fig. 11.

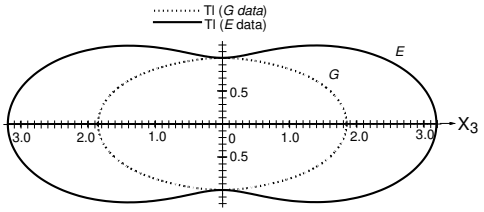

Figure 11. Normalized polar diagrams of La showing both E and G behaviour (direction of X_3 runs left to right.)

Figure 12 shows the modulus behaviours of Os, Pr, Tm, Hf; Ho, Ru and Tb, Dy Gd.

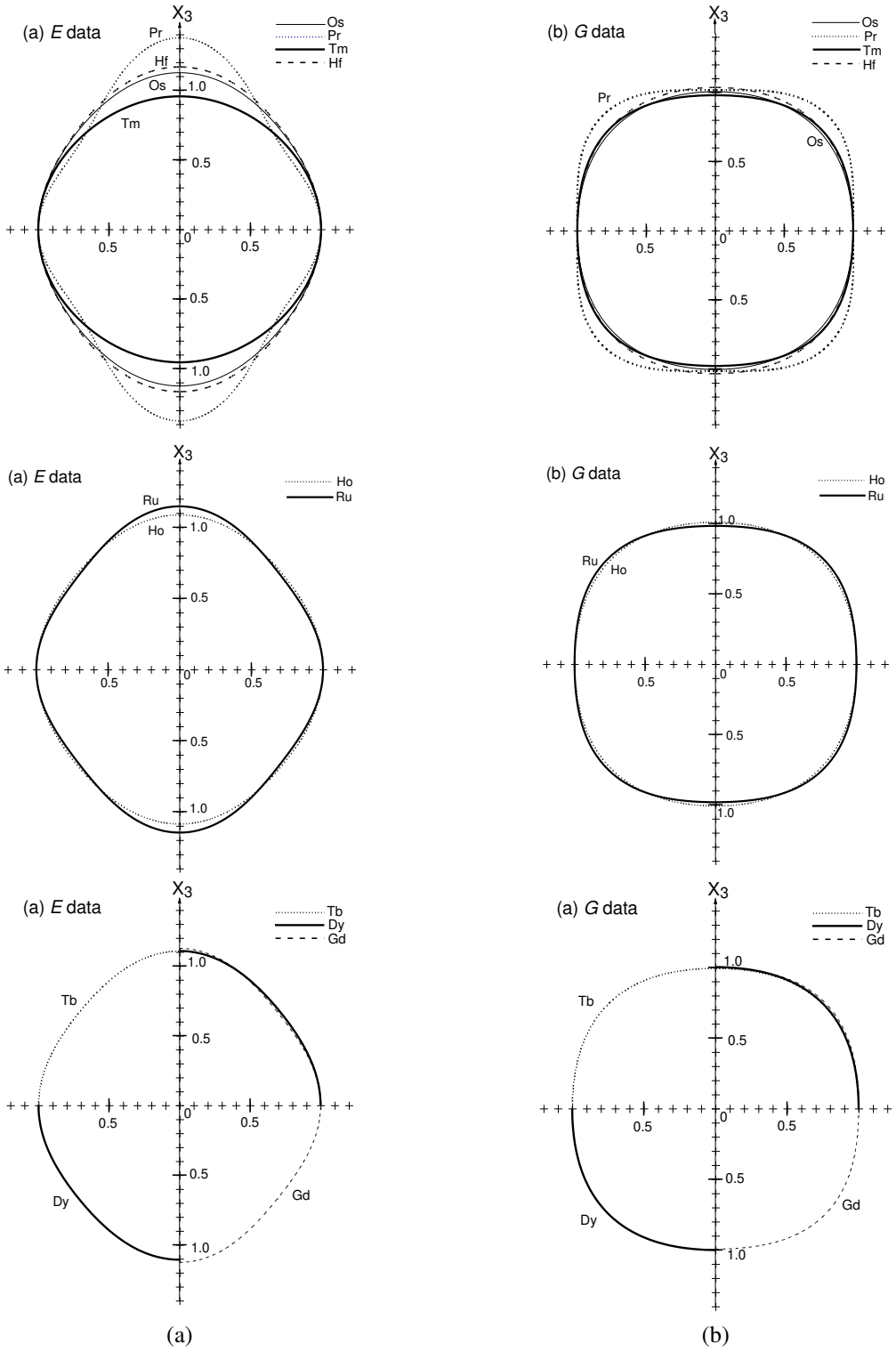

Figure 12. Normalized polar diagrams: Os, Pr Tm Hf, (top);). Ho, Ru (middle) and Tb, Dy, Gd (bottom) .(a) E data: (b) G data.

In the group Os, Pr, Tm and Hf, it is Tm which exhibits the most isotropic *E* and *G* behaviour. The least isotropic is Pr with a pronounced distorted circle in the X_3 direction. The normalised anisotropic behaviours of Ho and Ru are almost identical despite the large differences in the moduli of each metal (*c.f.* Figs. 7 and 8). The normalized values of the moduli for the metals Gd, Tb and Dy are virtually indistinguishable. In fact they are so similar that in both the

E and *G* polar diagrams, the upper right quadrant is a superposition of the data for all three metals, whereas the lower right quadrant is Gd data, the lower left quadrant is Dy data and the upper left quadrant is Tb data.

3. 7 Anisotropy Factors.

Based on the cylindrical symmetry of the polar diagrams around the X_3 axis in Figs. 9-12 it appears that the most practical and useful way of defining an anisotropy factor for each metal crystal is the ratio of the elastic moduli (reciprocal compliances) in the X_3 and X_1 directions, as shown in Eq. (18), based on Eqs. (10) and (12):

$$f_E = S_{11}/S_{33}\ ;\ f_G = (S_{44} + 2S_{11} - 2S_{12})/2S_{44} \tag{18}$$

The resulting anisotropy factors are listed in Table 6 utilising compliances listed in Table 2. It is evident that Tl is the most anisotropic metal, closely followed by Zn and Cd, with decreasing anisotropy in the general order Ti, Co, Pr, Nd, Zr, Re, and Be. Generally, the f_G values tend to indicate that the shear modulus exhibits less anisotropy than the tensile modulus. [N.B. Tomé [1998] discusses other means of expressing anisotropy in terms of stiffness constants.]

Table 6. Anisotropy factors f_E and f_G for hexagonal metals

Metal	f_E	f_G	Metal	f_E	f_G
Be	1.202	1.107	Nd	1.277	0.997
Mg	1.117	0.988	Gd	1.126	0.995
Sc	1.179	0.965	Tb	1.105	0.992
Ti	1.406	1.165	Dy	1.107	1.001
Co	1.402	1.022	Ho	1.087	1.009
Zn	0.293	0.796	Er	1.068	1.002
Y	1.072	0.999	Tm	0.955	0.978
Zr	1.273	0.977	Lu	0.966	0.995
Ru	1.148	0.983	Hf	1.166	1.034
Cd	0.361	0.765	Re	1.241	0.969
La	1.151	0.907	Os	1.125	1.004
Pr	1.377	1.015	Tl	3.286	1.851

4. POLYCRYSTAL BEHAVIOUR

In this section some methods are examined for estimating elastic moduli in a quasi-isotropic polycrystal aggregate composed of randomly oriented grains whose size is small relative to the size of the polycrystal, followed by comments on the influence of preferred orientation on polycrystal moduli.

4.1 Estimation of Polycrystal Moduli *E* and *G*.

4.1.1 .Average spherical modulus.

The behaviour of a completely randomly oriented aggregate of grains may be estimated from the compliances (*S*) by determining an average tensile modulus (E_{av}), and average shear modulus (G_{av}), based on a three dimensional summation of the angular variations of S'_{33} and S'_G in Eqs. (13) and (14)), subsequently termed the average spherical modulus. Calculations may be conducted in two ways. The first determination of E_{av} and G_{av} is based on the summated average of *N* moduli obtained from the reciprocal compliances as indicated in Eq. (19):

$$\begin{aligned}(E_{av})_1 &= (1/N)\left\{\sum_{n=1}^{n=N}[(1/S'_{33})_{n=1} + (1/S'_{33})_{n=2}\ldots\ldots + (1/S'_{33})_{n=N}]\right\}\\ (G_{av})_1 &= (1/N)\left\{\sum_{n=1}^{n=N}[(1/S'_{G})_{n=1} + (1/S'_{G})_{n=2}\ldots\ldots + (1/S'_{G})_{n=N}]\right\}\end{aligned} \tag{19}$$

The second determination of E_{av} and G_{av} is based on the reciprocal of the summated total of *N* compliances:

$$\begin{aligned}(E_{av})_2 &= (1/N)\left\{\sum_{n=1}^{n=N}1/[(S'_{33})_{n=1} + (S'_{33})_{n=2}\ldots\ldots + (S'_{33})_{n=N}]\right\}\\ (G_{av})_2 &= (1/N)\left\{\sum_{n=1}^{n=N}1/[(S'_{G})_{n=1} + (S'_{G})_{n=2}\ldots\ldots + (S'_{G})_{n=N}]\right\}\end{aligned} \tag{20}$$

Although Eqs. (19) and (20) are both calculated from compliances (tensors), the essential difference between them is that Eq. (19) is dependent upon the average of a summated set of reciprocal tensors whereas Eq. (20) involves the reciprocal average of a set of summated tensors. Obviously if the individual grains (crystals) were perfectly isotropic Eqs. (19) and (20) would yield identical results.

The calculation procedures for Eq. (19) involve a numerical integration of polar diagrams based on the reciprocal compliances $(S'_{33})^{-1}$ and $(S'_G)^{-1}$ which is described with reference to the θ *versus E* polar diagram of Fig. 13, using the Sc diagram in Fig 10 as an example. The integration is relatively straightforward because three dimensional polar diagrams of HCP crystals exhibit cylindrical symmetry around the X_3 axis. Consequently, all planes containing the X_3 axis are identical in shape and all planes normal to the X_3 axis are circular in shape but of different radius. Finally, all planes lying above the origin normal to the X_3 axis are mirror images of corresponding planes equidistant below the origin. Hence, the upper part of the polar diagram is a mirror image of the lower part.

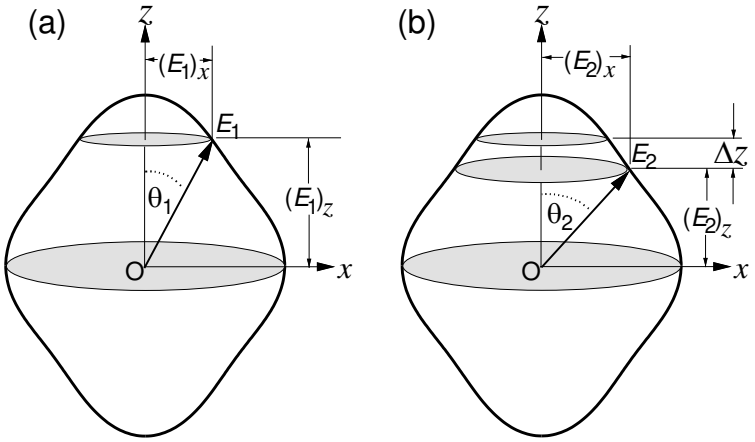

Figure 13. Polar diagram of Sc illustrating numerical integration procedures; z-axis equivalent to the X_3 axis.

Consider a modulus vector E_1 (*i.e.* $1/S'_{33}$) making an angle θ_1 with the *z*-axis in Fig 13(a), where the z-axis is equivalent to the X_3 axis in Fig. 10. The vector components on the *x* and *z* axes are $(E_1)_x = E_1\sin(\theta_1)$ and $(E_1)_z = E_1\cos(\theta_1)$, respectively. A second modulus vector E_2 in Fig.13(b) makes an angle θ_2 with the *z*-axis with vector components $(E_2)_x = E_2\sin(\theta_2)$ and $(E_2)_z = E_2\cos(\theta_2)$ on the *x*-axis and *z*-axis, respectively. If both vectors are rotated 360° around the *z*-axis two circles are formed of radius $(E_1)_x$ and $(E_2)_x$ which enclose a disc shaped volume of average radius $[(E_1)_x + (E_2)_x]/2$ and thickness $\Delta z = [(E_1) - (E_2)_z]$ Thus, if θ is allowed to increase from 0 to π radians (*i.e.* 180°) in small increments of Δθ (~one degree) the total volume V_E of the three dimensional polar diagram is the summation of a series of disc shaped volumes:

$$V_E \approx \frac{\pi}{4}\sum_{\theta=0}^{\theta=\pi}[(E_1)_z - (E_2)_z][(E_1)_x + (E_2)_x]^2 \tag{21}$$

The average radius $(E_{av})_1$ of an equivalent sphere of volume V_E is readily obtained:

$$(E_{av})_1 = \{3V_E/4\pi\}^{1/3} = \left\{\left(\frac{3}{16}\right)\sum_{\theta=0}^{\theta=\pi}[(E_1)_z - (E_2)_z][(E_1)_x + (E_2)_x]^2\right\}^{1/3} \tag{22}$$

The value of $(E_{av})_1$ in (22) is equivalent to $(E_{av})_1$ in Eq. (19) and calculated results are listed in Table 7. In like manner, $(G_{av})_1$ in Eq. (19) is obtained from the polar diagram of *G* (*i.e.* $1/S'_G$) using the same numerical integration procedures to obtain a spherical average $(G_{av})_1$ via Eq. (23), and the resulting values included in Table 7

$$(G_{av})_1 = \{3V_G/4\pi\}^{1/3} = \left\{\left(\frac{3}{16}\right)\sum_{\theta=0}^{\theta=\pi}[(G_1)_z - (G_2)_z][(G_1)_x + (G_2)_x]^2\right\}^{1/3} \tag{23}$$

Subsequently, the values of $(E_{av})_2$ and $(G_{av})_2$ in Eq. (20) were determined from polar diagrams of the compliance vectors S'_{33} and S'_G, using similar numerical integration procedures to those described for Eqs. (22) and (23) to obtain the average compliance radius, $(S'_{33})_{av}$ and $(S'_G)_{av}$, of a sphere having the same volume as the three dimensional polar diagram of compliances. Thus, $1/(S'_{33})_{av} = (E_{av})_2$ and $1/(S'_{44})_{av} = (G_{av})_2$, and their values are

listed in Table 7, together with the mean average spherical modulus $E_{mean} = [(E_{av})_1 + (E_{av})_2]/2$ and $G_{mean} = [(G_{av})_1 + (G_{av})_2]/2$. Note that a comparison of Tables 6 and 7 indicates that metals with anisotropy factors exhibiting the largest deviations from unity also tend to have the largest differences between $(E_{av})_1$ and $(E_{av})_2$, and between $(G_{av})_1$ and $(G_{av})_2$ (e.g. Zn, Cd and Tl).

Table 7. Polycrystalline modulus estimations based on spherical averages.

Metal	$(E_{av})_1$ (Gpa)	$(E_{av})_2$ (GPa)	E_{mean} (GPa)	$(G_{av})_1$ (GPa)	$(G_{av})_2$ (GPa)	G_{mean} (GPa)	ν_{mean}	K_{mean} (GPa)
Be	313.10	309.9	311.49	150.50	150.2	150.33	0.036	111.9
Mg	44.58	44.4	44.50	17.27	17.2	17.25	0.290	35.3
Sc	77.54	76.9	77.20	30.44	30.3	30.36	0.271	56.2
Ti	114.60	111.7	113.17	42.81	42.5	42.65	0.327	108.9
Co	202.50	198.1	200.29	75.75	75.1	75.43	0.328	193.7
Zn	109.15	73.3	91.20	38.04	34.2	36.13	0.262	63.9
Y	63.06	62.9	62.99	25.32	25.3	25.30	0.245	41.2
Zr	97.28	96.1	96.67	36.25	36.1	36.17	0.336	98.4
Ru	475.95	474.0	474.97	190.78	190.5	190.62	0.246	311.5
Cd	66.06	50.7	58.36	22.10	21.3	21.72	0.344	62.3
La	41.14	40.4	40.78	16.52	16.3	16.44	0.241	26.2
Pr	37.82	37.1	37.44	14.58	14.5	14.52	0.289	29.6
Nd	41.75	41.2	41.48	16.18	16.1	16.13	0.285	32.2
Gd	54.61	54.4	54.51	21.64	21.6	21.62	0.260	37.9
Tb	56.35	56.2	56.28	22.37	22.3	22.36	0.259	38.9
Dy	62.26	62.1	62.19	25.00	25.0	24.98	0.245	40.6
Ho	65.16	65.1	65.11	26.38	26.4	26.37	0.235	40.9
Er	69.95	69.8	69.90	28.20	28.2	28.18	0.240	44.8
Tm	73.46	73.14	73.30	29.51	29.7	29.59	0.238	46.7
Lu	68.44	68.4	68.42	27.15	27.1	27.15	0.260	47.6
Hf	143.06	142.4	142.73	55.63	55.6	55.59	0.284	110.0
Re	460.76	455.1	457.92	177.63	176.5	177.09	0.293	368.6
Os	675.65	673.9	674.75	275.24	274.8	275.02	0.227	411.6
Tl	16.67	12.0	14.35	4.77	4.4	4.58	‡0.565	Invalid
Tl			*12.0			*4.4	*0.364	*14.7

‡Invalid value, ν must be <0.5. *Based on assumption that $(E_{av})_2$ and $(G_{av})_2$ play dominant roles.

For an isotropic material the Poisson ratio ν and the bulk modulus K are given by standard relationships in Eq. (24) [e.g. see Hibbeler, 1997]:

$$\nu = \frac{E}{2G} - 1; \quad K = \frac{E}{3(1-2\nu)} = \frac{EG}{(9G - 3E)} \tag{24}$$

Based on E_{mean} and G_{mean} values, the Poisson ratio and bulk modulus calculated from Eq. (24) are included in Table 7, from which it is evident that sensible values are obtained for all metals except Tl where they are invalid (*i.e.* ν is > 0.5 and K is negative). This is perhaps not too surprising considering the large anisotropy factors for Tl in Table 6. Therefore $(E_{av})_2$ and $(G_{av})_2$ must play the more dominant roles in determining the spherical behaviour of Tl. Consequently, if E_{mean} and G_{mean} are replaced by $(E_{av})_2$ and $(G_{av})_2$ the Poisson ratio and bulk modulus of Tl exhibit sensible values, as shown on the last line of Table 7.

4.1.2 .Voigt and Reuss Analyses.

Commencing with the pioneering studies of Voigt in 1889 there has been ongoing interest in determining a general numerical relationship between monocrystal elastic constants of all crystal classes and the moduli of their respective quasi-isotropic polycrystal aggregates. Voigt [1889] based his analysis on the stiffness constants C_{mn} and the assumption that homogeneous strain was maintained throughout the stressed poly crystal in all directions (also see summary on pages 962-963 in Voigt [1928]). In this manner, via three dimensional integration, he derived general equations applicable to all crystal classes for two moduli; (i) the bulk modulus K involving volume change without shape change, and (ii) the shear modulus G which involves shape change without volume change. The value of

Young's modulus *E*, involving both shape and volume change was obtained by rearrangement of Eq. (24) applicable to isotropic materials *i.e.* $E_V = (G+3K)/9KG$. The general forms of the resulting moduli are shown in Eq. (25) using the subscript *V* to denote Voigt's analysis;

$$K_V = (c+2c_1)/3; \quad G_V = c_2; \quad E_V = (c_2)(c+2c_1)/(c_1+c_2) \tag{25}$$

where $c = (3A+2B+4\Gamma)/5$; $c_1 = (A+4B-2\Gamma)/5$; $c_2 = (A-B+3\Gamma)/5$; $c_2 = (c-c_1)/2$

$3A = C_{11}+C_{22}+C_{33}$; $3B = C_{23}+C_{31}+C_{12}$; $3\Gamma = C_{44}+C_{55}+C_{66}$.

After substituting for c, c_1, c_2, *A*, *B* and Γ, together with the six independent elastic stiffness constants for hexagonal crystal structures in Eq. (8), the HCP polycrystal moduli are obtained in terms of the C_{mn} in Eq. (26) and listed in Table 8:

$$\begin{aligned} K_V &= (A+2B)/3 = (2C_{11}+C_{33}+4C_{13}+2C_{12})/9 \\ G_V &= (A-B+3\Gamma)/5 = (3.5C_{11}+C_{33}-2C_{13}-2.5C_{12}+6C_{44})/15 \\ E_V &= \frac{(A-B+3\Gamma)(A+2B)}{(2A+3B+\Gamma)} = \frac{(3.5C_{11}+C_{33}-2C_{13}-2.5C_{12}+6C_{44})(2C_{11}+C_{33}+4C_{13}+2C_{12})}{3(4.5C_{11}+2C_{23}+6C_{13}+2.5C_{12}+2C_{44})} \end{aligned} \tag{26}$$

In a later study, Reuss [1929] calculated the bulk elastic modulus *K* and the shear modulus *G* of a polycrystal based on the compliances S_{mn} and the assumption that homogeneous stress was maintained throughout the stressed poly crystal in all directions. This analysis, involving a three dimensional integration, was examined by Hill [1952] and Gebrande [1982] and shown to lead to Eq. (27) applicable to all classes of crystals where the subscript *R* refers to the Reuss analysis:

$$K_R = 1/(3\alpha+6\beta); \quad G_R = 5/(4\alpha-4\beta+3\lambda): \quad E_R = (9K_RG_R)/(3K_R+G_R) \tag{27}$$

and $3\alpha = S_{11}+S_{22}+S_{33}$; $3\beta = S_{23}+S_{31}+S_{12}$: $3\lambda = S_{44}+S_{55}+S_{66}$.

After substituting for α, β, and λ in Eq. (27), together with the six independent compliances for hexagonal crystal structures in Eq. (8), the HCP polycrystal moduli are obtained in terms of the S_{mn} in Eq. (28), and listed in Table 8:

$$\begin{aligned} K_R &= 1/(2S_{11}+S_{33}+4S_{13}+2S_{12}) \\ G_R &= 15/(14S_{11}+4S_{33}-8S_{13}-10S_{12}+6S_{44}) \\ E_R &= 15/(8S_{11}+3S_{33}+4S_{13}+2S_{44} \end{aligned} \tag{28}$$

Table 8. Results of Voigt (V) and Reuss (R) analyses of moduli (K, G, and E)and combined Voigt-Reuss (V-R) averages.

Metal	K_V (GPa)	G_V (GPa)	E_V (GPa)	K_R (GPa)	G_R (GPa)	E_R (GPa)	$K_{V\text{-}R}$ (GPa)	$G_{V\text{-}R}$ (GPa)	$E_{V\text{-}R}$ (GPa)	$\nu_{V\text{-}R}$
Be	111.67	151.80	313.39	110.99	150.27	310.62	111.33	151.0	312.0	0.033
Mg	35.23	17.36	44.73	35.26	17.24	44.48	35.25	17.3	44.6	0.289
Sc	55.84	30.85	78.15	55.90	30.34	77.07	55.87	30.6	77.6	0.268
Ti	105.00	44.20	116.28	105.26	42.59	112.58	105.13	43.4	114.4	0.319
Co	187.44	78.27	206.11	187.27	75.32	199.26	187.36	76.8	202.7	0.320
Zn	72.67	46.61	115.20	59.45	35.31	88.43	66.06	41.0	101.8	0.243
Y	41.23	25.49	63.40	41.12	25.29	62.96	41.18	25.4	63.2	0.244
Zr	96.67	36.76	97.87	96.25	36.14	96.36	96.46	36.4	97.1	0.332
Ru	310.89	191.63	476.91	310.95	190.56	474.71	310.92	191.1	475.8	0.245
Cd	59.21	25.67	67.28	48.83	21.58	56.42	54.02	23.6	61.8	0.309
La	25.96	16.95	41.76	25.95	16.41	40.65	25.95	16.7	41.2	0.235
Pr	28.82	15.05	38.46	28.84	14.50	37.26	28.83	14.8	37.9	0.281
Nd	31.79	16.53	42.27	31.78	16.12	41.36	31.78	16.3	41.8	0.281
Gd	37.85	21.75	54.75	37.86	21.62	54.49	37.86	22.0	54.6	0.241
Tb	38.81	22.43	56.41	38.76	22.35	56.25	38.79	22.4	56.3	0.258
Dy	40.53	29.07	70.38	40.52	24.98	62.16	40.53	27.0	66.3	0.226
Ho	40.87	26.45	65.27	40.85	26.36	65.09	40.86	26.4	65.2	0.234
Er	44.68	28.32	70.13	44.52	28.18	69.81	44.60	28.2	70.0	0.239
Tm	46.39	29.91	73.86	45.77	29.69	73.25	46.08	29.8	73.6	0.234
Lu	47.70	27.16	68.48	47.60	27.15	68.43	47.65	27.2	68.5	0.261
Hf	108.56	56.01	143.38	108.58	55.58	142.44	108.57	55.8	142.9	0.281
Re	365.00	180.70	465.31	365.50	176.90	456.98	365.25	178.8	461.1	0.290
Os	412.22	275.53	675.99	411.56	274.84	674.40	411.89	275.2	675.2	0.227
Tl	36.26	6.20	17.61	36.34	4.49	12.94	36.30	5.3	15.3	0.428

Hill [1952] concluded that both the Voigt and Reuss were approximations because the forces between the grains could not be in equilibrium with Voigt's [1889] assumption of constant strain, whereas in the Reuss [1929] model the distorted grains could not fit together under the assumption of homogeneous stress. Hence, from a consideration of the energy densities, Hill [1952] determined that the Voigt moduli (E_V and G_V) should exceed the Reuss moduli

(E_R and G_R), consistent with Table 8, and the true values should lie between these two bounds. This led to Hill (1952) suggesting a mean value between the two could be a good approximation. Consequently, the mean values (Voigt+Reuss)/2 are listed in Table 6 with subscripts *V-R*. (N.B. The calculated $K_{V\text{-}R}$ for diamond is ~458 GPa, based on Hearmon's [1979] elastic constants. This compares with a $K_{V\text{-}R}$ of ~412 GPa for Os. Hence, osmium has an elastic hardness approaching diamond and much interest has been shown in the similarity and difference in compressibility (reciprocal *K*) between the two elements [Hebbache and Zemzemi 2004]).

Comparison of Tables 7 and 8 shows that there is a generally good agreement between the E_{mean}, G_{mean} and K_{mean} moduli obtained via the spherical analysis method and the mean $E_{V\text{-}R}$, $G_{V\text{-}R}$ and $K_{V\text{-}R}$ moduli obtained via the Voigt-Reuss analyses. The exception is Tl where, even though the E_{mean} and G_{mean} values are comparable to the $E_{V\text{-}R}$, and $G_{V\text{-}R}$, the ν_{mean} and K_{mean} are invalid.

Other analyses of note concerning polycrystal behaviour are those by Huber and Schmid [1934] and Boas and Schmid [1934]. Their analyses are more complex to use than those of Voigt [1889] in Eq. (26)) and by Reuss [1929] in Eq. (28). However, the results of Boas and Schmid [1934] indicate their *E* and *G* values for Mg, Zn and Cd are near to and slightly less than those obtained by the Voigt analysis. Ledbetter [1990] has provided critical comment on these and lesser used methods to estimate randomly oriented polycrystal behaviour. Overall, it appears that the most useful procedures are the Voigt-Reuss analyses combined with Hill's [1952] averaging method.

4.1.3 Polycrystal *C* and *S* matrices.

For a truly random aggregate of grains the HCP monocrystal matrices in equation (8) should be replaced by isotropic matrices which have only two independent stiffness constants and two independent compliances [Nye, 1985] as indicated in Eq. (29):

$$\begin{bmatrix} C_{11} & C_{12} & C_{12} & \bullet & \bullet & \bullet \\ C_{12} & C_{11} & C_{12} & \bullet & \bullet & \bullet \\ C_{12} & C_{12} & C_{11} & \bullet & \bullet & \bullet \\ \bullet & \bullet & \bullet & C_{44} & \bullet & \bullet \\ \bullet & \bullet & \bullet & \bullet & C_{44} & \bullet \\ \bullet & \bullet & \bullet & \bullet & \bullet & C_{44} \end{bmatrix} \quad \begin{bmatrix} S_{11} & S_{12} & S_{12} & \bullet & \bullet & \bullet \\ S_{12} & S_{11} & S_{12} & \bullet & \bullet & \bullet \\ S_{12} & S_{12} & S_{11} & \bullet & \bullet & \bullet \\ \bullet & \bullet & \bullet & S_{44} & \bullet & \bullet \\ \bullet & \bullet & \bullet & \bullet & S_{44} & \bullet \\ \bullet & \bullet & \bullet & \bullet & \bullet & S_{44} \end{bmatrix} \tag{29}$$

$$C_{44} = (C_{11} - C_{12})/2 \qquad S_{44} = 2(S_{11} - S_{12})$$

Clearly, $1/G = S_{44} = 2(S_{11}\text{-}S_{12})$, and since $S_{11} = 1/E$, then $S_{12} = (1/E)\text{-}(1/2G)$ and the stiffness constants may be obtained via matrix inversion. This been done, based on the $E_{V\text{-}R}$ and $G_{V\text{-}R}$ moduli in Table 8, and the results listed in Table 9.

Table 9. Compliance and stiffness constants for polycrystals having a randomly oriented aggregate of grains.

Metal	S_{11} $(TPa)^{-1}$	S_{12} $(TPa)^{-1}$	S_{44} $(TPa)^{-1}$	C_{11} (GPa)	C_{12} (GPa)	C_{44} (GPa)
Be	3.21	-0.11	6.62	312.71	10.64	151.04
Mg	22.42	-6.49	57.80	58.36	23.76	17.30
Sc	12.88	-3.46	32.69	96.66	35.47	30.59
Ti	8.74	-2.78	23.04	162.95	76.17	43.39
Co	4.93	-1.58	13.02	289.69	136.10	76.80
Zn	9.82	-2.38	24.41	120.59	38.67	40.96
Y	15.83	-3.87	39.39	75.03	24.25	25.39
Zr	10.30	-3.42	27.44	145.05	72.15	36.45
Ru	2.10	-0.51	5.23	565.69	183.49	191.10
Cd	16.17	-5.00	42.34	85.51	38.27	23.62
La	24.27	-5.71	59.96	48.19	14.83	16.68
Pr	26.41	-7.42	67.67	48.52	18.97	14.78
Nd	23.92	-6.71	61.26	53.54	20.90	16.32
Gd	18.31	-4.75	46.12	66.76	23.40	21.68
Tb	17.75	-4.58	44.66	68.64	23.86	22.39
Dy	15.09	-3.41	37.00	76.37	22.32	27.02
Ho	15.34	-3.59	37.87	76.07	23.25	26.41
Er	14.29	-3.41	35.40	82.26	25.77	28.25
Tm	13.60	-3.18	33.55	85.82	26.21	29.80
Lu	14.61	-3.81	36.83	83.85	29.55	27.15
Hf	7.00	-1.96	17.92	182.96	71.37	55.80
Re	2.17	-0.63	5.59	603.61	246.01	178.80
Os	1.48	-0.34	3.63	778.81	228.43	275.19
Tl	65.48	-28.03	187.03	42.55	31.85	5.35

4.2 Preferred Orientation.

In practice, it is difficult to obtain an ideally randomly oriented crystalline aggregate. Initial departures from randomness may occur during solidification due to differences in crystal growth directions. Subsequent metal working processes, such as rolling, extrusion, annealing and recrystallization, provide other mechanisms for the formation of preferred orientation textures. Typical textures developed during metal processing of HCP metals have been discussed by Rollet and Wright [1998] and Wang and Huang [2003]. Examples of studies on specific metals include those on Be [Brown et al. 2005], Zn [Solas *et al*. 2001], Mg [Agnew *et al* 2001], Gehrmann *et al*.2005], and Ti [Balasubramanian and Anand 2002, and Zaefferer 2003]. In general, much work has been conducted on the effects of processing temperature and plastic deformation modes (slip and twinning) on texture development, especially for the control of directional ductility and yield stress in engineered products. Little experimental information is available on the anisotropic elastic behaviour of textured polycrystals and when preferred orientation effects are present the Voigt-Reuss analyses for complete randomness in Table and 8 are of are of limited application.

Based on the polar diagrams in Figs. 9 to 12 and the anisotropy factors in Table 6, it is possible to make some general comments on the effects of texture on elastic anisotropy of HCP polycrystals. First, the metals with polar diagrams which most approach circularity with an anisotropy factor close to unity should experience smaller directional variations in the resulting elastic moduli, *E* and *G,* as result of metal processing. These include Mg and Y. In contrast, metals with significant departures from circularity, and anisotropy factors much less or greater than unity, are likely to experience considerable directional variations in their elastic moduli as a result of processing. In particular, these include Zn and Cd. Important metals such as Be, Ti Zr and Co are likely to experience some variations in their polycrystal moduli, but not to the same extent as Zn and Cd.

If a strong texture is present it is possible to anticipate some elastic anisotropy effects. Extruded rods of hexagonal metals such as pure Ti often exhibit a cylindrical symmetry fibre texture where the basal plane poles (*i.e*. [0001]) of the grains are perpendicular to the extrusion axis [Rollet and Wright, 1998]. Consequently the tensile modulus along the extrusion axis E_{axis} should approach that of the modulus normal to the prismatic planes of the monocrystal ~$1/S_{11}$ (~104 GPa from Table 2). Cold rolling textures in sheet metals such as Zn and Cd with c/a ratios >1.633 tend to have the basal poles [0001] tilted ± 15° to 25° from the normal to the rolling plane (RP) towards the rolling direction (RD) and $[11\bar{2}0]$ poles aligned with the RD [Rollet and Wright 1998]. Consequently, Young's modulus E_{TD} in the transverse direction (TD) should approach that on the prismatic planes of the monocrystal (*i.e*. $1/S_{11}$) and E_{RD} should approach that of a plane whose normal is inclined ~70° to the X_3 axis of the monocrystal (see Figs 5 and 6, and Eq. 13). The shear modulus G_{RP} on the RP should approach that of a plane whose normal is inclined ~20° to the X_3 axis of the monocrystal (see Fig. 6 and Eq. (14). Resulting estimated values of E_{TD}, E_{RD} and G_{RP} are listed in Table 10.

Table 10. Estimated moduli of cold rolled textured sheet.

Metal	E_{TD} (GPa) (GPa)	E_{RD} (GPa) (GPa)	G_{RP} (GPa) (GPa)	E_{TD}-$E_{V\text{-}R}$ (GPa)	E_{RD}-$E_{V\text{-}R}$ (GPa)	G_{RP}-$G_{V\text{-}R}$ (GPa)
Zn	124	127.7	36.8	+22.2	+25.9	-4.2
Cd	82.0	74.5	19.2	+20.2	+12.7	-4.4
Mg	45.4	45.4	16.4	+0.8	+0.8	-0.9
Co	200.4	200.4	71	-2.3	-2.3	-5.8
Zr	91.5	98.1	36.7	-5.6	+1.0	+0.3
Ti	108.8	104	45.8	-5.6	-9.4	+2.4
Hf	139.3	139.9	56.9	-3.6	-3.0	+1.1

Cold rolling of Metals with *c/a* ratio close to the ideal value of 1.633, such as Mg and Co in Table 1, tends to form [0001] textures where the basal plane lies in the RP [Rollet and Wright 1998]. Consequently, both E_{TD} and E_{RD} should approach the modulus on the prismatic planes of the monocrystal, $1/S_{11} = 1/S_{22}$, and G_{RP} should approach the shear modulus on the basal plane, $1/S_{44}$. The resulting values are listed in Table 10. For metals with c/a ratios such as Zr, Ti and Hf , with *c/a* ratios <1.633, the basal poles are tilted ±20 to 40 degrees away from the normal to the sheet by a rotation around the rolling direction (RD), where the [1010] poles coincide with the RD [Rollet and Wright 1998]. Consequently E_{RD} should approach that of the prismatic plane of the monocrystal (~$1/S_{11}$) and E_{TD} should correspond to that of a plane whose normal is tilted ~60° from the X_3 direction in Fig. 7. The G_{RP} should correspond to a plane whose normal is tilted ~ 30° from the X_3 direction. Estimated values are listed in Table 10. The differences between the estimated texture moduli and the corresponding Voigt-Reuss (*V-R*) in Table 8 are also listed in Table 10.

It is evident from Table 10 that the influence of texture on elastic moduli is most pronounced for Zn and Cd, significant for Ti, somewhat significant for Co, Zr, Ti and Hf, and least for Mg. The magnitude of the differences in moduli produced by texture effects in Table 10 are within the ranges of experimental study via sensitive dynamic modulus measurements [Wolfenden 1990]. Such techniques could be usefully applied more widely to the study of preferred orientation and texture development.

5. CONCLUSIONS

As a group, the HCP metals cover a wide range of atomic numbers and exhibit a broad spectrum of elastic properties extending from low shear modulus (G) and low Young's modulus (E) to high G and E values, together with a range of bulk moduli varying from the elastically soft (low K) to the elastically hard (high K). The cylindrical symmetry of the HCP crystal structure lends itself well to the calculation and graphical representation of the anisotropic dependence of monocrystal E and G moduli on crystallographic direction. The anisotropic elastic behaviour of the monocrystal exerts its influence on the elastic behaviour of polycrystals and, under well characterized preferred orientation (texture) conditions, the anisotropy of E and G in the textured polycrystal may be estimated.

6. ACKNOWLEDGEMENTS

The author wishes to thank the Natural Sciences and Engineering Research Council (NSERC) of Canada for financial support of the study.

7. REFERENCES

[1]. Agnew S.R., Yoo M.H. Tomé C.N., 2001. *Application of texture simulation to understanding mechanical behaviour of Mg and solid solution alloys containing Li or Y.* Acta mater. **49**, pp 4277-4289.

[2]. Balasubramanian S., Anand L., 2002. *Plasticity of initially textured hexagonal polycrystals at high homologous temperatures: application to titanium.* Acta mater. **50**, 133-148.

[3]. Baughman R.H., Shacklette J.M., Zakhidov A.A., Stafström S., 1998. *Negative Poisson's ratios as a common feature of cubic metals.* Nature **392**, pp 392-365.

[4]. Blessing, G.V. 1990. *The pulsed ultrasonic velocity method for determining material dynamic elastic moduli.* A. Wolfenden (Ed.), Dynamic Elastic Modulus Measurements in Materials, STP 1045, ASTM, Philadelphia PA, pp 47-57.

[5]. Boas W., Schmid E. 1934. *Zur Berechnung physikalischer Konstanten quasiisotroper Vielkristalle*. Helvetica Phys. Acta, **7**, pp 628-632.

[6]. Brown D.B., Abeln S.P., Blumenthal W.R., Bourke M.A.M., Mataya M.C., Tomé C.N. 2005. *Development of crystallographic texture during high rate deformation of hot-pressed beryllium.* Met. Mat. Trans. A **36A**, pp 929-939.

[7]. Cullity, B.D., 1956. "Elements of X-Ray Diffraction", Addison-Wesley Inc., Reading, MA.

[8]. Dixon L.W., Papaconstantopoulos D.A., Mehl M.J., 2008. *Electronic structure and superconducting properties of lanthanum.* Phys. Rev. B **78**, pp 214510-1 to 214510-13.

[9]. Gebrande H., 1982. *Elasticity and inelasticity.* Hellwege, K.-H., and Angenheister (Eds.), Landolt-Börnstein Tables, Group V, Vol. 1, Springer-Verlag, Berlin, pp 1-96.

[10]. Gehrman R., Frommert M.M., Gottstein G., 2005. *Texture effects on plastic deformation of magnesium*. Mat. Sci. Eng. A **395**, pp 338-349.

[11]. Hearmon R.F., 1946. *The elastic constants of anisotropic materials*. Rev. Modern Phys. **12**(1), pp 409-440.

[12]. Hearmon R.F., 1979. *The elastic constants of crystals and other anisotropic materials.* In: Hellwege K.-H., Hellwege A.M. (Eds.), Landolt-Börnstein Tables, Group III, Vol. 11, Springer-Verlag, Berlin, pp 1-154.

[13]. Hebbache M., Zemzemi M., 2004. *Ab initio study of the high-pressure behaviour of a low compressibility metal and a hard metal: Osmium and Diamond*. Phys. Rev. B **70**, pp 224107-(1-6).

[14]. Hibbeler R.C.,1997. Mechanics of Materials, Prentice-Hall Inc., Upper Saddle River, NJ, USA.

[15]. Hill R., 1952. *The elastic behaviour of a crystalline aggregate.* Proc. Phys. Soc. A **65**, pp 349-354.

[16]. Huber, A., Schmid E., 1934. *Bestimmung der elastischen Eigenschaftsen quasiisotroper Vielkristalle durch Mittelung*. Helvetica Phys. Acta, **7**, pp 620-627.

[17]. Ledbetter H., 1990. *Monocrystal-polycrystal elastic constant models.* A. Wolfenden (Ed.), Dynamic Elastic Modulus Measurements in Materials, STP 1045, ASTM, Philadelphia PA, pp 135-148.

[18]. Lim C.M., Edwards C., Dixon S., Palmer S.B., 2001. J. Magnetism Magnetic Mat. **234**, pp 387-394.

[19]. Lubarda V.A., Meyers M.A., 1999. *On the negative Poisson ratio in monocrystalline zinc.* Scripta Mater. **40**(8), pp 975-977.

[20]. Metals Handbook, 1985. Desk Edition, H.E. Boyer and T.L. Gall (Eds.) ASM, Metals Park, OH, USA, pp 1-43 to 1-48.

[21]. Nareth, A.,1969. *Nuclear magnetic resonance in hexagonal lanthanum metal: Knight shifts, spin relaxation rates, and quadrupole coupling constants.* Phys. Rev. **179**(1), pp 359-368.
[22]. Nye, J.F., 1985. "Physical Properties of Crystals –Their Representation by Tensors and Matrices", Oxford University Press, UK.
[23]. Ouyang Y., Tao X., Zeng F., Chen H., Du Y., Feng Y., He Y., 2009. *First-principles calculations of elastic and thermo-physical properties of Al, Mg and rare earth lanthanide elements.* Physica B **404**, pp 2299-2304.
[24]. Pantea C., Stroe I., Ledbetter H., Betts J.B., Zhao Y., Daemen L.L., Cynn H., Miglion A., 2008. *Osmium's Debye temperature.* J. Phys. Chem. Solids **69**, pp 211-213.
[25]. Reuss, A., 1929. *Berechung der Fließenze von Mischkristallen auf Grund der Plastizitätsbedingung für Einkristalle.* Zeit. Angew. Math. Mech. (ZAMM), **9**, pp 49-58.
[26]. Rollett A.D., Wright S.I., (1998). *Typical textures in metals.* U.F. Kocks, C.N. Tomé, H.R. Wenk (Eds.), Texture and Anisotropy, University Press, Cambridge, UK, pp 178-238.
[27]. Rowland W.D., White J.S., 1972. *The determination of the elastic constants of beryllium in the temperature range 25 to 300^o C.* J. Phys. F: Metal Phys. **2**, pp 231-236.
[28]. Singh N., 1999. *Phase transformation and elastic constants of HCP rare earth metals: Theory.* Physica B **270**, pp 298-306.
[29]. Solas D.E., Tomé C.N., Engler O. Wenk H.R., 2001. *Deformation and recrysatallization of hexagonal metals modeling and experimental results for zinc.* Acta mater. **49**, pp 3791-3801.
[30]. Stassis C., Loong C.-K., Zaretsky J., 1982. *Phonon dispersion curves of fcc La.* Phys. Rev. B **26**(10), pp 5426-5432.
[31]. Tomé C., 1998. *Tensor properties of textured polycrystals.* U.F. Kocks, C.N. Tomé, H.R. Wenk (Eds.), Texture and Anisotropy, University Press, Cambridge, UK, pp 283-324.
[32]. Voigt, W., 1889. *Ueber die Beziechung zwischen den beiden Elasticitätsconstanten isotroper Körper.* Ann. d. Phys. u. Chem. N.F. **38**, pp 573-587.
[33]. Voigt, W., 1928. "Lehrbuch Der Kristallphysik", B.G. Teubner, Leipzig, Germany.
[34]. Wang, Y.N., Huang, J.C., 2003. *Texture analysis in hexagonal materials.* Mater. Chem. Phys. **81** pp 11-26.
[35]. Weil R., Lawson A.W., 1966. *Ultrasonic studies in normal and superconducting thallium.* Phys. Rev. **141**(1) pp 452-460.
[36]. Wolfenden A, 1990. (Ed.) Dynamic Elastic Modulus Measurements in Materials, STP 1045, ASTM, Philadelphia, PA.
[37]. Wooster W.A., 1949. "A Textbook on Crystal Physics", Cambridge University Press, UK.
[38]. Yeganeh-Haeri A., Weidner D.J., Parise J.B., 1992. *Elasticity of α-cristobalite: A silicon dioxide with a negative Poisson's ratio.* Science, **257**(July), pp 650-652.
[39]. Zaefferer S., 2003. *A study of active deformation systems in titanium alloys: dependence on alloy composition and correlation with deformation texture.* Mat. Sci. Eng., **A344** pp 20-30.